THERMORESPONSIVE POLYPEPTOID IRON OXIDE CORE-SHELL NANOPARTICLES

Barbara Pretzner

Institute for Biologically Inspired Materials

Department of Nanobiotechnology

University of Natural Resources and Life Sciences, Vienna

This thesis is submitted for the degree of Master of Science

April 2017

To:

My partner, my parents and all of my great friends for their enormous support.

Thank you!

KURZFASSUNG

Auf thermische Reize ansprechende Polypeptoide finden Dank ihrer Biokompatibilität ein breites Anwendungsspektrum im biomedizinischen Bereich. Werden diese mittels der grafting-from Methode von superparamagnetischen Eisenoxid-Nanopartikeln (SPION) polymerisiert, wird ein System erzeugt, welches eine temperaturabhängige Löslichkeit sowie magnetische Extraktion kombiniert. In dieser Masterarbeit wird die Synthese und Analyse von dicht gepackten Core-Shell Nanopartikeln diskutiert, deren kolloidale Stabilität mittels thermischer Reize bestimmt werden kann. Es wurde bereits an thermisch-reaktiven Polypeptoiden geforscht, jedoch wurden diese von flachen Oberflächen und nicht von SPION mittels der grafting-from Methode polymerisiert. Die aufwendige Synthese der sehr empfindlichen Monomere und die beschränkte Verfügbarkeit an monodispersen, superparamagnetischen Eisenoxid-Nanopartikeln erschweren die Forschung auf diesem Gebiet.

Die Masterarbeit kann in die die Synthese der Monomere und deren Polymerisation von den Initiator-modifizierten SPION, um Co-Polypeptoid modifizierte Core-Shell Eisenoxid-Nanopartikeln herzustellen, unterteilt werden. Der erste Abschnitt der Thesis behandelt die Herstellung von *N*-Methyl- und *N*-Butyl-*N*-Carboxyanhydrid mittels zwei verschiedenen Synthesewegen, wobei sich eine modifizierte Fuchs-Farthing Methode durch eine höhere Monomer-Reinheit und -Ausbeute als bessere Option bewiesen hat.

Der zweite Teil beschäftigt sich mit der Polymerisation von Co-Polypeptoiden von Initiator-modifizierten SPION. Verschiedenen Verhältnisse an *N*-Methyl- und *N*-Butyl-*N*-Carboxyanhydrid wurden für die Ringöffnungspolymerisation unter inerter Atmosphäre eingesetzt, um die thermische Reaktivität der Polymere zu variieren. Mehrere Reaktionsparameter wie Lösungsmittel, Reaktionsdauer und Reaktionstemperatur wurden getestet und diskutiert. Kolloidal stabile, thermisch-reaktive, monodisperse Co-Polypeptoid-modifizierte SPION wurden hergestellt, aufgereinigt und mittels dynamischer Lichtstreuung, Kernspinresonanzspektroskopie, thermogravimetrischer Analyse, Transmissions-elektronenmikroskop und Matrix-Assistierte Laser-Desorption-Ionisierung mittels Flugzeitanalyse analysiert. Damit dieses hergestellte System für biomedizinische Zwecke eingesetzt werden kann, muss die komplexe Zusammensetzung des thermischen Verhaltens der Co-Polypeptoide weiter erforscht und die Polymerisationsbedingungen optimiert werden.

ABSTRACT

Thermoresponsive polypeptoids offer a wide variety of opportunities for biomedical applications due to their biocompatibility. Grafted from superparamagnetic iron oxide nanoparticles (SPION), a system can be obtained that combine a temperature-triggered solubility transition with magnetic extraction. In this master thesis the synthesis and analysis of densely grafted core-shell nanoparticles with tunable thermoresponsive colloidal stability is discussed. Research was already done on thermoresponsive polypeptoids grafted from flat surfaces, but has never been investigated by the grafting from approach on SPION. The laborious synthesis of the highly reactive monomers and the limited access to monodisperse, superparamagnetic iron oxide nanoparticles hampers intensive research on this topic.

This master thesis can be divided into two parts comprising the synthesis of monomers and their polymerization from initiator-modified SPION to generate co-polypeptoid modified core-shell iron oxide nanoparticles. In the first part of the thesis the synthesis of *N*-Methyl- and *N*-Butyl-*N*-carboxyanhydride by two different approaches is discussed, whereby a modified Fuchs-Farthing method proved to lead to a higher yield and higher purity than Leuchs' method.

In the second part different ratios of *N*-Methyl- and *N*-Butyl-*N*-carboxyanhydride were used for ring opening polymerization of the co-polypeptoid from initiator-modified iron oxide nanoparticles under inert atmosphere. Varying ratios of the monomers lead to co-polypeptoids with different thermal behavior. Several polymerization conditions such as solvents, polymerization duration and reaction temperature were tested. Colloidally stable, thermoresponsive, monodisperse co-polypeptoid modified SPIONs could be obtained and were purified and investigated by dynamic light scattering, nuclear magnetic resonance, thermogravimatric analysis, transmission electron microscopy and matrix assisted laser desorption ionization – time of flight mass spectrometry. To be useful for biomedical applications, more research is needed to understand the complex composition of the thermal behavior and to optimize polymerization conditions for full control over synthesis of the co-polypeptoid.

ACKNOWLEDGEMENTS

My biggest thanks goes to my supervisor Univ. Prof. Dr. Erik Reimhult, who welcomed me at his department, gave me the chance to work for this project, introduced me to the scientific world, taught me a lot about nanotechnology and always provided thought-provoking impulses. His sarcasm and knowledge about indie movies led often to fun and interesting conversations.

For his patience to teach me chemistry, I would like to thank Dipl.-Ing. Dr. Ronald Zirbs, who co-supervised my master thesis and taught me how to survive in the lab. His expertise in chemistry, pleasant demeanor, good sense of humor and open ear for my problems made him to a very great and congenial co-supervisor.

A big thanks goes to Dipl.-Chem. Dr. Steffen Kurzhals, who taught me how to analyze MALDI-TOF MS and complex ^{1}H-NMR results, helped me with experiments, always gave me good input when writing my thesis and provided me with helpful feedback.

I also thank M. Sc. Martina Schroffenegger, for being such a great colleague, supporting me with her chemistry knowledge, withstanding my whining about my failed experiments and last but not least for the many laughs we shared.

For supporting me with monodisperse iron oxide nanoparticles, I would like to thank B. Sc. Tanja Zwölfer, who untiringly synthesized the particles in high quality.

Furthermore I would like to thank M. Sc. Noga Gal, Dipl.-Ing. Iris Vonderhaid, B. Sc. Max Willinger and all the other great people at this department for being such fun and pleasant colleagues. They supported me with their encouraging words and laughs even outside the lab.

Finally I want to thank Stephanie, my parents and especially my friends for not being angry with me, when I was preoccupied with my thesis.

CONTENTS

1 INTRODUCTION

The exceptional properties of core-shell nanoparticles (CSNP) and their composition is discussed in this chapter. Furthermore the following paragraphs provide the reader with the necessary knowledge and concepts for better understanding of this ingenious, biologically inspired material topic.

1.1 Core-Shell Nanoparticles

The word “nano” received more and more attention in the media over the last few decades. However nanomaterials are not new. Humans have been exposed to nanoparticles since the beginning of our existence. Dust, aerosols or viruses are just a few examples of nano-sized materials. Materials which are at least in one dimension between 1 and 100 nanometers are called nanomaterials [1]. On this length scale quantum mechanical effects play a major role which influence the matter’s optical [2], electronic [3] or mechanical properties. In the last decades microscopic and scattering techniques have advanced enormously [4]. This technical progress enables the characterization and analysis of nanomaterials.

Biological inspired engineering of materials combine biological principles with other sciences such as physics or chemistry. This fusion of different scientific areas lead to new engineering solutions for medicine, industry, environmental issues and many other fields. CSNP are a novel outcome of this scientific discipline. Such smart materials, which can response to external changes like heat, pH or light, have attracted much attention in research lately [5]. Especially thermoresponsive polymers, changing their structure when exposed to temperature change, are particular useful in science [6]. When combined with superparamagnetic, monodisperse nanoparticles (NPs), a wide range of medical, biological and technological applications are feasible. Zhang and his research group have conducted intensive research on drug delivery with CSNP. In 2007 they synthesized magnetic drug-targeting carrier consisting of ferromagnetic nanoparticles encapsulated with a smart polymer [7]. The scope of application in the biomedical field and the improvement of this novel system encourage further study.

CSNP usually consist of two different materials, schematically shown in Figure 1. The interplay of the core and the shell is based on different close interactions. Depending on the combination

of the arranging materials, CSNP can be divided in following classes: inorganic/inorganic, organic/organic, inorganic/organic or organic/inorganic. The choice of these four systems is depending on the application's use [8].

Figure 1: 3D presentation of the core/shell concept. The green sphere represents the shell and the blue sphere shows the inner core.

The research done in this master thesis concentrates on an inorganic/organic or hard/soft CSNP system. Where iron oxide is chosen for the inorganic and polymer for the organic material.

1.1.1 Structure of Core-Shell Nanoparticles

When talking about inorganic/organic CSNP approaches, the structure can be broken down into three simple parts: core, anchor and spacer. Figure 2 gives a graphical impression of how the structure of a CSNP can be assembled.

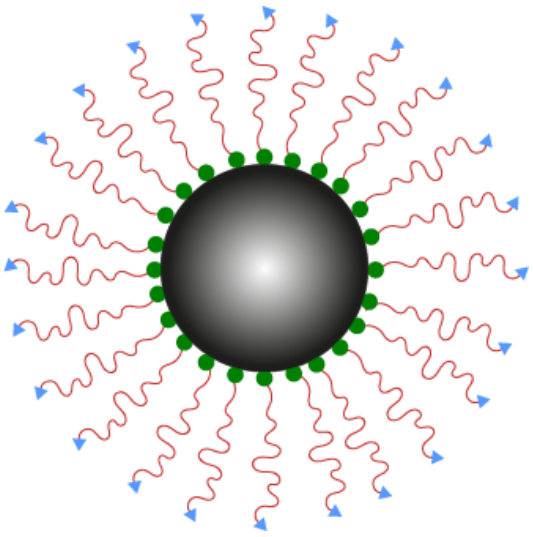

Figure 2: Sketch of CSNP system: the black sphere as the solid core, the green small spheres as anchors, the red lines as spacers and the blue triangles as functional groups.

The core is the solid phase of the system where anchor and spacer is bound to. To keep the NPs dispersed, a spacer (shell) needs to be densely attached to the core's surface to provide colloidal stability. Unfortunately the core cannot simply be covered with the shell, but has to be modified prior coating. The surface modification of the NP implies the attachment of a suitable and strongly bound anchor. The detailed description of the three parts can be found in the following sections.

1.2 Iron Oxide Nanoparticle - Core

Different materials, such as silica, gold or iron oxide can be used as core materials for CSNPs. Furthermore the choice of the inorganic substance also strongly, apart from the method of synthesis, influences the shape of the NP, shown in Figure 3.

Figure 3: Three different shapes of CSNPs: (a) spherical CSNP; (b) hexagonal (crystalline) CSNP; (c) multiple core materials coated by a single shell material.

Superparamagnetic iron oxide nanoparticles (SPIONs) are a good choice of smart material, when it comes to usage in biomedical field [9], as contrast agents [10] and especially in drug delivery [11]. Superparamagnetism allows that magnetization can be randomly flipped by induced thermal energy and only occurs in sufficiently small, monocrystalline ferromagnetic NPs. When superparamagnetic NP are influenced by an external magnetic field, the NP reacts similar to a paramagnet [12]. In case when the superparamagnetic NP interacts with an alternating magnetic field, the flipping of the magnetization direction with respect to the magnetic crystal grain boundary leads to dissipation of the magnetic energy as heat. To obtain monocrystalline SPIONs, they should not exceed a core size above 15 nm. The biocompatibility of SPIONS is due to the reason, that iron oxide breaks down to Fe^{3+} under acidic conditions such as in the human stomach [10]. The degraded iron can be used in the human body which makes Fe_3O_4 NPs biocompatible. The resulting size of the NP strongly depends on the used synthesis method. In general it can be said that the complex process for producing NPs can be classified in physical (gas phase deposition, electron beam lithography, aerosol, powderball milling), chemical (microemulsion, electrochemical deposition, sonochemical, thermal decomposition, hydrothermal, coprecipitation) or biological (fungi, bacteria or protein mediated) methods [13].

In the process of synthesizing iron oxide NPs with monodisperse size distribution a capping agent (also called surfactant or ligand) has proved very helpful. Such small NPs will aggregate immediately due to their interactions with themselves or with biological molecules without a surfactant shell. The capping agent acts as spacer between the NPs and prevents agglomeration. This master thesis was provided with SPIONs by the Department of Nanobiotechnology (BOKU) according to the protocol of *Hyeon et. al.*[14], synthesized by Tanja Zwölfer (B. Sc.). Monodisperse iron nanoparticles are synthesized by a reaction with ironpentacarbonyl and oleic acid (OA) in dioctylether at high temperature. Oleic acid serves as surfactant against agglomeration. Furthermore the ratio of OA to iron oxide has a big influence on the resulting size of the SPION [15]. To coat the NPs with the desired initiator, a ligand exchange has to be performed. OA has proven to be very persistent to be replaced. Remaining OA residues are a big issue, since every impurity decreases the grafting density of the polymer shell and therefore the colloidal stability as well [15].

1.3 Nitrodopamine – Anchor

An anchor is indispensable when it comes to connect an inorganic (hard) material with an organic (soft) one. In the best case the anchor has a high binding affinity and a very low desorption rate. Commercially available iron oxide NP used for clinical applications are usually coated with dextran, alginate or poly(acrylic acid) (PAA). These dispersants have a very high molecular weight and lack high affinity anchors that could bind the polymer irreversible to the NP surface. Such polymer shells often encapsulate multiple cores which results in huge clusters. This in enlargement would make the CSNPs impractical for many drug delivery applications, such as passive targeting by the enhanced permeation and retention effect [9].

Erik Reimhult et. al. investigated catechol-derivate anchor groups which possess irreversible binding affinity to iron oxide [16]. They found out that especially 6-nitrodopamine (Figure 4) is a suitable candidate as anchor. The molecule forms a very stable complex with Fe^{3+} due to its bidentate catechol ligands and allows diluting and heating of iron oxide nanoparticle suspension without agglomeration [17].

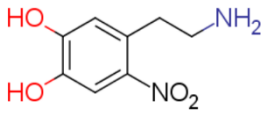

Figure 4: Chemical structure of 6-nitrodopamine.

This small molecule acts as anchor and initiator for the in-situ polymerization of the spacer at the same time. The packing density of bound nitrodopamine on the NP determines the brush density and therefore the stability of the CSNP. The anchor is synthesized prior their adsorption to the NP. After manufacturing, the ligand exists as a 6-nitrodopamine hemisulfate [18]. To start the polymerization the hemisulfate is removed by adding *N*-Methyl-2-pyrrolidone (NMP) to enable a nucleophilic attack by the amine group of the nitrodopamine. A graphical impression of how the anchor is linked to the SPION is shown in Figure 5. The detailed protocol for this process can be found in the supporting information of Bixner *et. al.* [15].

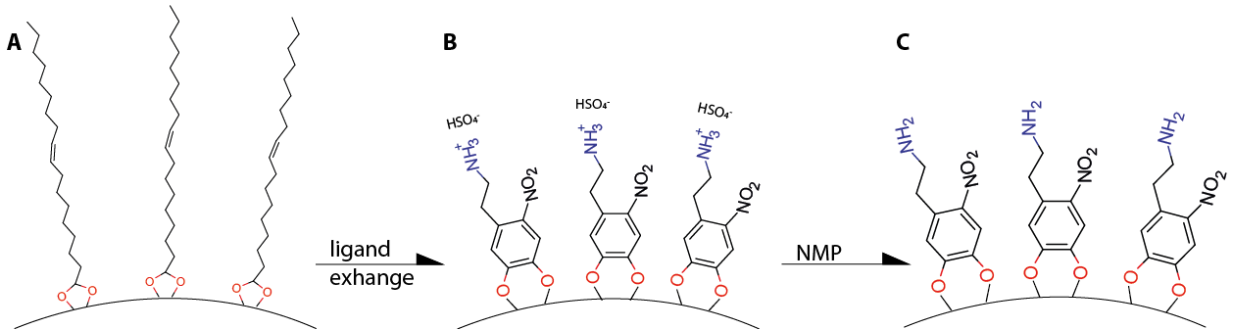

Figure 5: Section of the surface of a SPION with different surface modifications; (A) SPION modified with OA as capping agent; (B) SPION modified with 6-nitrodopamine hemisulfate after ligand exchange; (C) SPION modified with 6-nitrodopamine after adding NMP.

1.4 Polypeptoid – Shell

Nanoparticles have a very high surface to volume ratio, their interaction with the environment is mainly determined by their interface. Chemistry offers a wide variety of potential polymers, consisting of organic monomers, for coating nanoparticles. The polymer's main tasks include functionality, colloidal stability and biocompatibility. When SPIONs are used for biomedical application the choice of polymer is quite limited. Bio-inspired polymers are a good option if biocompatibility is desired.

Polypeptoids, consist of repeating *N*-substituted glycine units and can close the gap between natural and fully synthetic molecules [19]. The polypeptoids covered in this master thesis are derived from living ring-opening polymerization of *N*-carboxy anhydrides (NCAs). Their biocompatibility is attributable to their degradable aliphatic backbone structure. These nature inspired polymers are structurally very similar to natural peptides, except that the side chain is bound to the nitrogen and not to the backbone structure, displayed in Figure 6 [20].

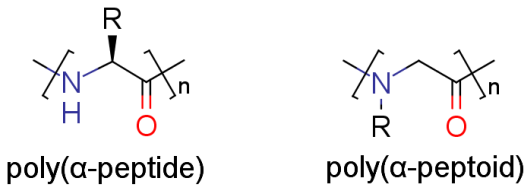

Figure 6: Chemical structure of polypeptides and polypeptoids.

Over the last decade the controlled polymerization of polypeptoids in terms of molecular weight, architecture and composition has highly improved [21]. Further the polypeptoid is not just a simple repetition of amino acids but can build secondary structures. Unlike peptides, α-polypeptoids do not have a chiral center nor remarkable hydrogen-bonding interactions [20]. However the side chain of the polyamino acid has a huge influence on its secondary structure and can lead to α-helices [22] or β-sheet assembling [23]. By variation of the individual monomers used for the polymerization the polypeptoid's thermo-responsiveness can be altered. All these features and possible modifications offers synthetic, structural and functional adaptability. Especially responsive nanomaterials can benefit of these advantages. Furthermore the morphology of a polymer brush is influenced by the interaction between the polymer chains and the solvent.

1.4.1 Polymer Composition and Lower Critical Solution Temperature

Besides being biocompatible and offering many architectural possibilities, the α-polypeptoids discussed in this thesis are also thermoresponsive in water. Other polymers that exhibit thermoresponsive behavior in water include poly(*N*-isopropylacrylamide) (PNIPAM) [24] and polyoxazolines [25]. It has been investigated that the cloud point temperature (T_{CP}) of thermo-responsive polypeptoids can be changed with its chain length, end-group structures, molecular weight and concentration [26]. The molecular weight can be altered by the feed ratio of monomers to initiator. By changing the composition of the polypeptoid, such as using different ratios of *N*-Methyl - and *N*-Butyl-NCA, the transition temperature can be adjusted [27]. Other research groups investigated the tunable lower critical solution temperature (LCST) values of co-polypeptoids polymerized from *N*-Ethyl-NCA and *N*-Butyl-NCA, obtaining LCST values between 25 – 80 °C [26]. The knowledge of the influence of each parameter on the LCST is still very limited. Below the LCST the polymer is completely soluble in water. Above this critical temperature the α-polypeptoid changes its interaction with the solvent from hydrophilic

to hydrophobic, depictured in Figure 7, and undergoes a hydrophobic collapse. This leads to aggregation and precipitation of the polypeptoid.

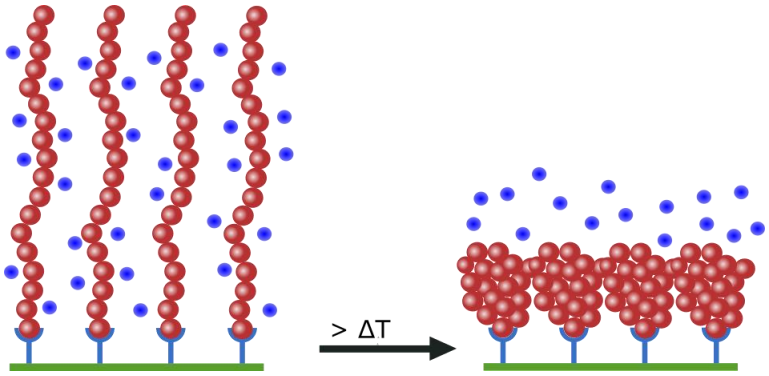

Figure 7: Scheme of thermo-responsive polymer brush: below LCST (soluble, hydrated) on the left and above LCST (aggregated, dehydrated) on the right side. The blue dots display H_2O molecules which get excluded, if the LCST is reached.

1.4.2 Surface Grafting of Polypeptoids

To guarantee colloidal stability of the SPIONs the polymer chains need to be in close proximity to each other to obtain a brush regime, depicted in Figure 8. With sufficient proximity the free volumes of the chains overlap. Unfavorable interactions are avoided when the gap between each chain is smaller than their radius of gyration (R_G) [28].

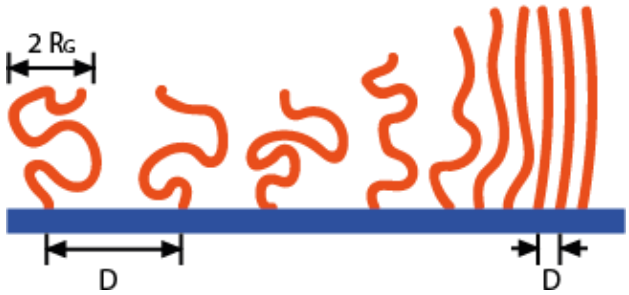

Figure 8: Transition between mushroom regime $D > 2R_G$ and brush regime $D < 2R_G$.

Furthermore the brush regime is controlled by chain length and chemical composition of the polymer. The morphology of a diluted polymer brush is influenced by the interaction between the polymer chains and the solvent. Tethered polymer appear in a mushroom shape when the chains are not interacting with each (Figure 9). When the chain interaction with the substrate is higher than with the solvent, the polymer appears in a pancake regime.

Figure 9: Mushroom regime on the left side, pancake regime on the right side.

In general there are two methods to attach covalently bound polymers to a solid substrate. Pre-synthesized polymer chains can be grafted to the substrate (grafting to) or the polymer is directly grown from the surface (grafting from).

Grafting-To Method

The grafting-to approach involves the chemical reaction of pre-synthesized, functionalized polymer with surfaces containing complementary functional groups (Figure 10)[29]. For example corresponding materials can be: gold/sulfur, silane/hydroxyl groups or Fe_3O_4/nitrodopamine

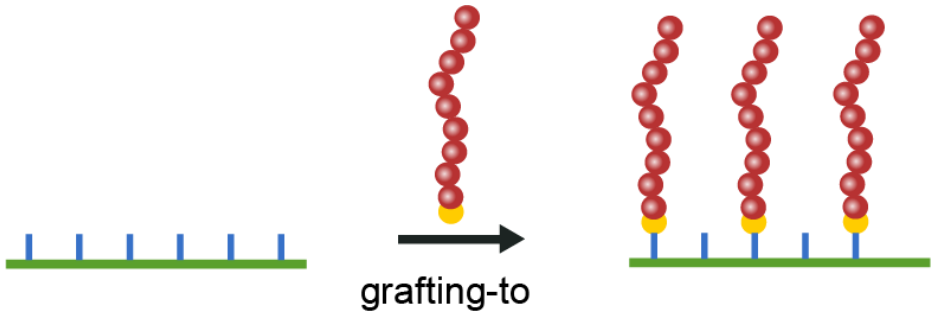

Figure 10: Scheme of attachment of an end-functionalized (yellow sphere) polymer (red chain) on a modified flat surface (green and blue figures).

The advantage of this method is that the polymer can be easily pre-synthesized in a separate process and allows full characterization prior the assembly to the surface. This approach is commonly chosen when a brush regime on a flat surface is desired. Grafting densities of 0.87 chains per nm^{-2} are possible with polysarcosine grafted to flat titanium dioxide [30]. The downside of this technique is that the polymer brush density is lower than with the grafting-from method. Depending on the polymer's size its length can lead to entanglement or steric repulsion which hampers the attachment onto the surface and often results in the formation of non-homogeneous films with low grafting densities [31].

Grafting-From Method

An alternative to the grafting-to method is the polymer grafting to the surface by polymerization from an immobilized initiator (grafting-from). Anchoring an initiator to the substrate is essential for this approach. Polypeptoids are synthesized by the grafting-from method involving surface-initiated ring-opening polymerization (ROP) of NCAs [32] (Figure 11). Since the polymer is directly grown from the surface, the polymer density is not influenced by diffusion hindrance resulting in high grafting density.

This allows a grafting density of nearly 2 chains per nm^{-2} grafted from magnetite nanoparticles via controlled radical polymerization of benzyl methacrylate, as K. Babu and R. Dhamodharan report [33].

Figure 11: Scheme of a grafting-from polymerization on a modified surface (green and blue figure), yielding a higher brush (red chains) density than with the grafting-to method.

1.4.3 Monomers *N*-carboxyanhydrides

α-amino acid *N*-carboxyanhydrides are organic cyclic compounds, structurally related to amino acids and very well suited for living polymerization. This class of monomers is highly reactive providing high electrophilic reactivity at the carbonyl group of the α-amino acid which leads to instability in water causing immediate polymerization [34]. This property makes it extremely laborious to synthesize these monomers. High purity solvents and working under inert atmosphere are essential for synthesizing, since water molecules are ubiquitous.

NCAs were discovered by Hermann Leuchs in 1906 [35] and are nowadays an eminent reactant in organic and polymer synthesis. Leuchs synthesized the anhydride by heating *N*-ethoxycarbonyl amino acid chloride in vacuum at 50-70 °C, the chemical reaction is depicted in Figure 12.

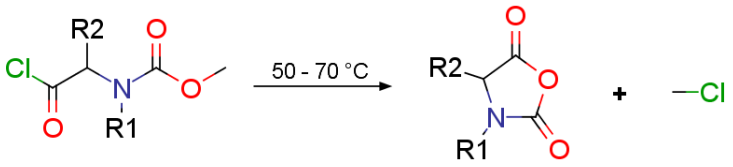

Figure 12: Synthesis of the original Leuchs anhydride.

High temperature caused decomposition of a great amount of the monomer which resulted in a very low yield. However, over the years many research groups developed and improved the synthesis of NCAs [27, 36]. Some of these improved methods were used for this master thesis and are described in chapter 4.1. There is a wide variety of NCAs (Figure 13) with different substitutes depending on the CO-activated amino acid used for synthesis.

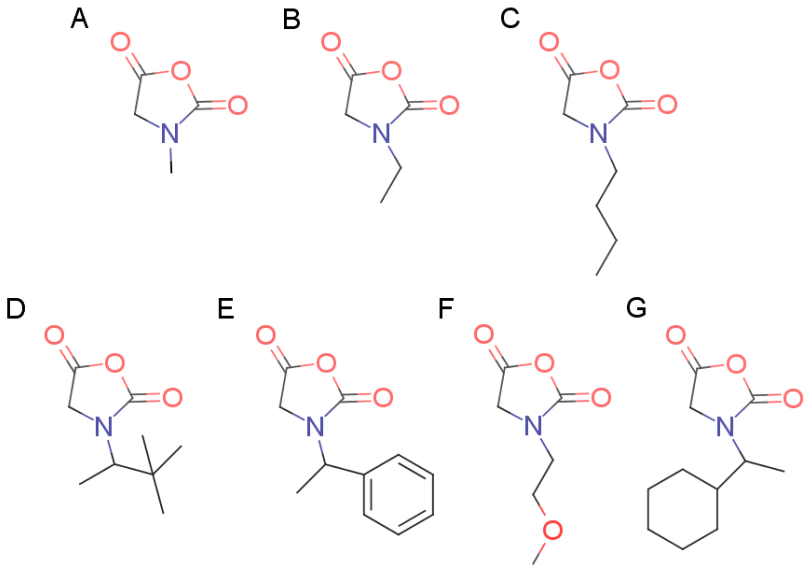

Figure 13: *N*-substituted *N*-carboxyanhydrides with different residues: A: *N*-methyl-NCA (Me-NCA), B: *N*-ethyl-NCA (Et-NCA), C: *N*-butyl-NCA (Bu-NCA), D: *N-(1,2,2-trimethylpropyl)*-NCA, E: *N-(1-phenylethyl)*-NCA, F: *N-(2-methoxyethyl)*-NCA, G: *N-(1-cyclohexylethyl)*-NCA.

The side chain determines the architecture of the polypeptoid such as β-sheets (glycine, valine, isoleucine, serine, threonine and cysteine) [23], α-helices [22] (e.g.: leucine, phenylalanine and tryptophan) or random coils (polysarcosine) [37]. This wide range of building blocks offers the opportunity to create homo, cyclic or block copolymers. This master thesis concentrates on the synthesis of Me-, Bu- and Et-NCA for polymerization of co-polypeptoids with different thermoresponsive behavior. Adjusting the T_{CP} with monomers of different hydrophobicity is the most effective way for the corresponding copolymer. Polysarcosine has an excellent water-solubility and is miscible with water in all ratios. *N*-Ethylglycine has moderate solubility in water, whereas *N*-Butylglycine is almost insoluble in water [27]. Copolymerization of these monomers in different ratios tunes the LCST of the co-polypeptoid.

1.4.4 Ring-opening polymerization of *N*-carboxyanhydride

First attempts in synthesizing polypeptoids were done with initiating the ring-opening polymerization by using water, alcohols or primary amines with poor control over the polymerization. Deming was the first who reported on metal-catalyzed NCA-ROP with “living” polymerization characteristics in the 1950s, achieving well-defined high molecular weight of homo and co-polypeptoids [38]. The metal remains in the final polypeptoid, which is a major drawback when it comes to biocompatibility. Over the years the development of NCA-ROP enhanced by using novel initiators [39] and polymerization techniques [40]. However our α-polypeptoids are synthesized by a nucleophilic (anionic) ring-opening polymerization of NCAs

in solution [20]. The reaction can be initiated by using an initiator such as primary amines like benzylamine or nitrodopamine. To guarantee chain growth and to keep the living polymerization running a base such as *N*-Methyl-2-pyrrolidone (NMP) has to be added to the reaction. NMP is a weak base and deprotonates the end group of the growing chain which enables the binding of the next monomer. The free electron pair of the primary amine nitrogen attacks the carbon with the lowest electron density. This results in CO_2 elimination with every additional Leuchs anhydride [41]. The speed of polymerization can be enhanced by applying vacuum, by moving the equilibrium to the right side of the chemical reaction (Figure 14).

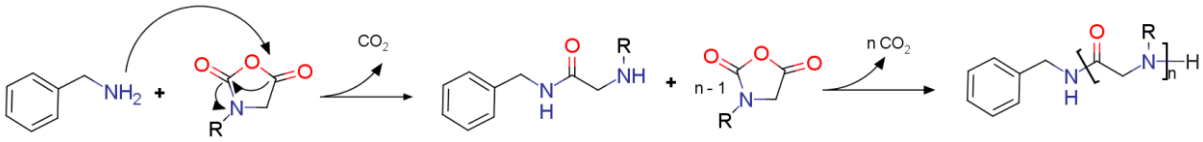

Figure 14: Initiation of polymerization with benzylamine, reaction mechanism according to Kricheldorf (Primary Amine).

Furthermore high vacuum technique (HVT) is used to maintain the conditions necessary for living polymerization such as keeping the reaction impurity-free [40]. However *Robert Luxenhofer et. al.* report that no correlation between Me-NCA kinetics and pressure could be observed [27].

Living polymerization is characterized by: full control over architecture, same end group on every polymer chain, fast initiation, low polydispersity and a predictable molecular weight (Figure 15). As long as the polymerization is not terminated, the chain growth keeps on going when fresh monomer is added. This enables the possibility of creating block copolymers and other polymers of complex architectures [42]. Not every monomer is suitable for this kind of polymerization which limits this technique tremendously. Nucleophilic contaminants (H_2O, amines or alcohols) in the reaction cause side products or termination of the polymerization. Due to this fact extremely pure solvents and monomers are essential to fulfill the conditions for this sensitive polymerization. Nevertheless, the possibility of control over the macromolecular synthesis and the precise composition of the polypeptoid makes this method attractive for novel material science.

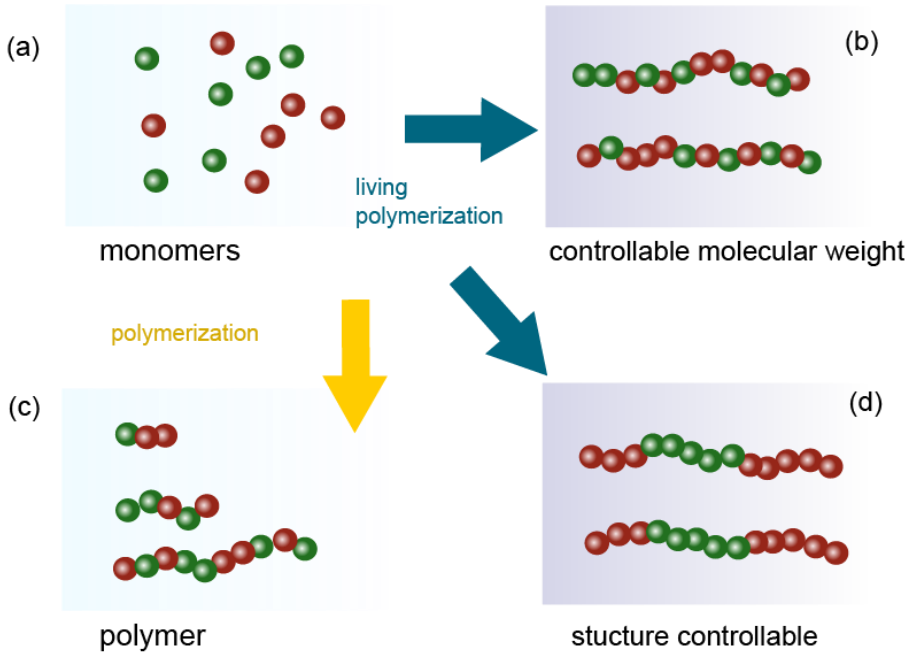

Figure 15: Scheme showing the difference between free and living polymerization. (a) shows two different kinds of monomers (green and red spheres). (c) displays the resulting polymer obtained by a free polymerization. (b) shows the product with living polymerization and the possibility to control the MW. (d) displays the polymer after living polymerization with a controlled structure.

1.5 Characterization of Core-Shell Nanoparticles

Before using SPIONs it is important to know their core size, efficiency of ligand exchange and the size distribution. For investigation of these parameters a combination of different analytical techniques is used. Transmission electron microscopy (TEM) shows the distribution and the core size of CSNPs and core-core agglomeration can be identified. Dynamic light scattering (DLS) provides information about the hydrodynamic diameter of dispersed NP, which is the actual NP size when dispersed in water with a hydrated shell. Furthermore T-cycled DLS measurements allow the characterization of the LCST for each CSNP sample. The packing density of the dispersant, ligand or polypeptoid-shell can be analyzed by thermogravimetric analysis (TGA). TGA heats the sample up until decomposition of the organic material is reached. The amount of material loss is used to calculate the grafting density on the nanoparticle.

2 AIM

The aim of this work was the synthesis and analysis of monodisperse, superparamagnetic, iron oxide nanoparticles with densely surface-grafted-from, co-polypeptoid shells – synthesized by ROP of Me- and Bu-NCA – that have tunable thermoresponsive colloidal stability, which is depicted in Figure 16.

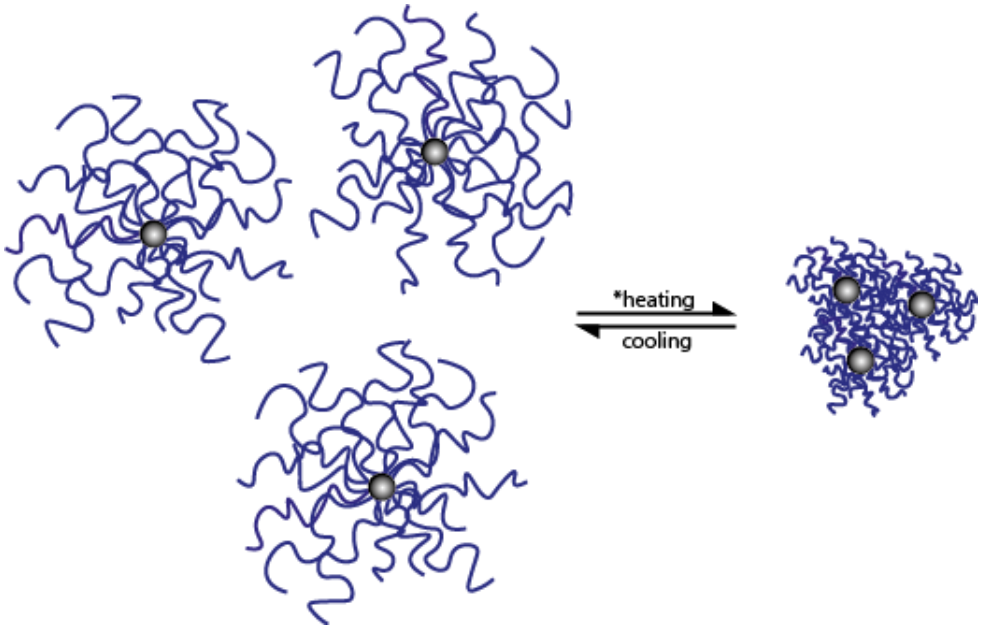

Figure 16: Schematic demonstration of thermoresponsive behavior of polymer-modified nanoparticles. * Local heating by magnetic field as well global thermal heating.

To achieve this goal following steps have to be taken:

I. Synthesis of monomers suitable for manufacturing biocompatible and thermoresponsive polymers.
II. Synthesis of thermoresponsive core-shell nanoparticle (CSNP) by surface-initiated polymerization of *N*-carboxyanhydrides from monodisperse SPION.
III. Investigation of the prepared core-shell nanoparticle with respect to their magnetic and thermoresponsive properties.

3 CONCEPT

The first step is to synthesize nanoparticles. Iron oxide nanoparticles have been proved to be an optimal choice as core material for biocompatible, thermoresponsive CSNP due to their biocompatibility and superparamagnetism. Monodisperse, spherical iron oxide nanoparticles are synthesized via high temperature thermal decomposition of ironpentacarbonyl in a high boiling oleic acid/dioctylether solution. Their purity, size and monodispersity is checked by TGA and TEM. During the synthesis of the core, oleic acid is used as capping agent to prevent particle agglomeration. Furthermore oleic acid achieves diffusion limited synthesis conditions, leading high monodispersity. The capping agent needs to be replaced to enable the binding of the initiator for polymerization on the core, depicted in Figure 17. 6-Nitrodopamine is chosen as initiator for polymerization which strongly binds to the core. After ligand exchange and purification of the SPION, the grafting density of the initiator is determined by TGA.

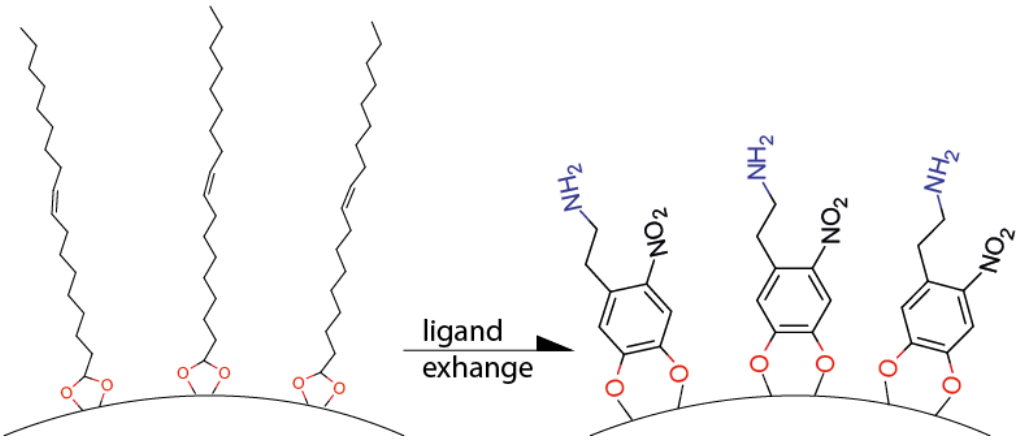

Figure 17: Section of a nanoparticle surface showing the exchange of oleic acid with nitrodopamine.

We chose two different *N*-carboxyanhydrides as monomers for polymerization due to their capability of forming biocompatible and thermoresponsive co-polypeptoids. *N*-carboxyanhydrides are highly reactive to nucleophilic molecules, therefore synthesis, purification and polymerization is done under inert atmosphere. The purity of the monomers is be analyzed by ^{1}H-NMR.

Co-polypeptoids with various lower critical solution temperature are polymerized containing different molar ratios of the monomers. The polymerization of polypeptoids from the iron oxide nanoparticle surface should be carried out in a glovebox using nitrodopamine-modified SPION, two different *N*-carboxyanhydrides, base and solvent (Figure 18).

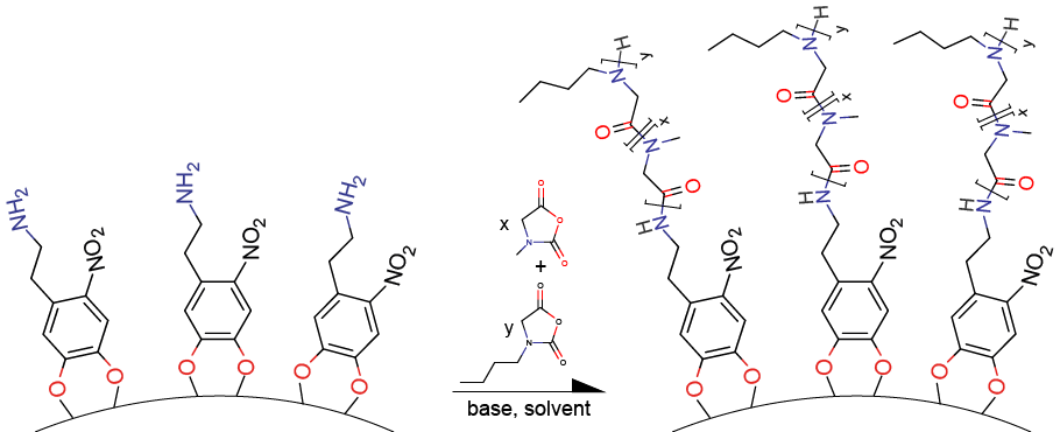

Figure 18: Section of a nitrodopamine-modified nanoparticle surface showing the polymerization of the co-polypeptoid.

Purification of the core-shell nanoparticles is required for further characterization of their properties. Grafting-density of the co-polypeptoid, differences in the lower critical solution temperature, hydrodynamic diameter, molecular weight, actual molar monomer fraction and colloidal stability is investigated by TGA, DLS, MALDI-TOF MS and TEM.

4 RESULTS AND DISCUSSION

This chapter presents the results of this master thesis. First, different methods for synthesis of the monomers are discussed and compared. Second, the polymerization of the prepared *N*-substituted NCAs is discussed in detail in terms of conditions, kinetics and characterization.

4.1 Monomer Synthesis

In general there are two options for synthesis: Fuchs-Farthing method and Leuchs' method (Figure 19). Method A, Leuchs' method, is based on the cyclization of *N*-alkoxycarbonyl amino acid halides to form α-amino acid *N*-carboxyanhydrides [43]. There are several approaches for Leuchs' method and research groups continue to develop these, since yield is still a problem. The substituent of the NCA-monomer influences not only the LCST or secondary structure of the formed polypeptoid, but also the melting point at room temperature. Therefore purification, such as distillation or sublimation, has to be adjusted to every individual monomer.

The Fuchs-Farthing method directly phosgenates the unprotected α-amino acid. This involves the handling with triphosgene. Since this chemical agent is highly hazardous, this kind of method is not further discussed in this thesis. However *Sisido et. al.* modified the Fuchs-Farthing method where phosphortrichloride (PCl_3) is used for ring closure [44], depicted in Figure 19. Phosphortribromide could also be used for the last step instead of PCl_3, but has never been carried out during this thesis. When synthesizing NCA, the carboxyl group of the intermediated molecule has to be covered with di-*tert*-butyldicarbonate or benzyl chloroformate to activate the ring closure during polymerization.

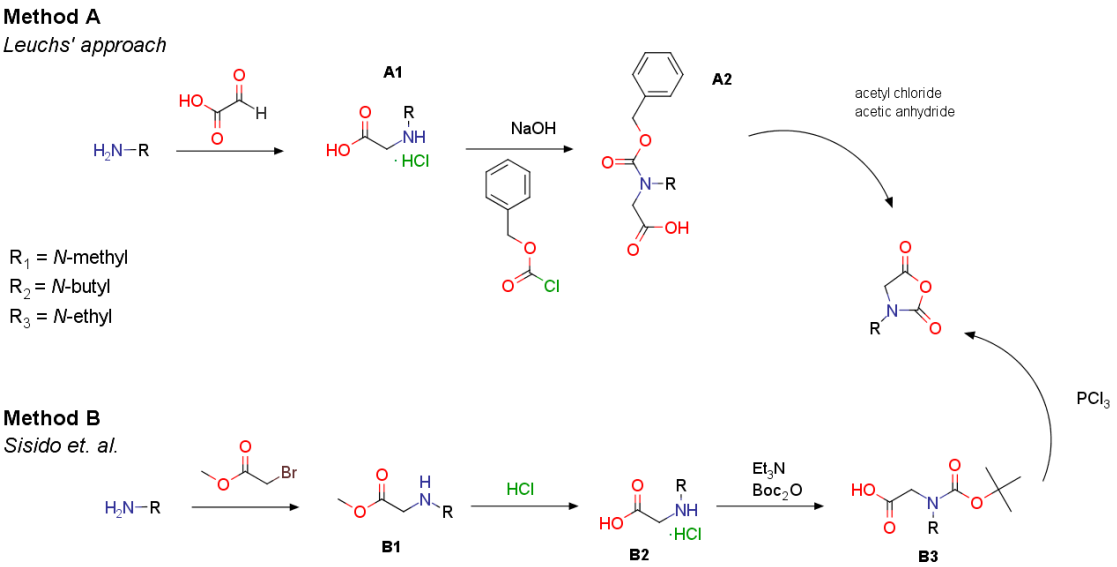

Figure 19: Overview diagram of two different mechanisms to synthesize *N*-substituted NCA. Method A shows Leuchs' approach where benzyl chloroformate is used as protective group. The modified Fuchs-Farthing method according to *Sisido et. al*. uses di-*tert*-butyldicarbonate (Boc_2O) as protective group (method B).

Both protective groups were tested and will be discussed in the individual monomer synthesis subchapters. When it comes to the ring-closure of the NCA the solvent has to be absolutely pure and the working atmosphere needs to be water free. For this reason the last step of the synthesis can only be done under inert atmosphere, like working inside a glovebox.

Table 1: Summary of the final products of monomer syntheses.

Entry	Abbreviation[b]	NCA	Method	Yield [%]
M1	BPR03	Methyl	A	30.05
M2	BPR49	Methyl	A	-[a]
M3	BPR55	Methyl	A	-[a]
M4	BPR57	Methyl	A	11.00
M5	BPR67	Methyl	B	20.36
M6	BPR69	Methyl	B	-[a]
M7	BPR71	Methyl	B	44.43
M8	BPR06	Butyl	A	-[a]
M9	BPR22	Butyl	B	-[a]
M10	BPR26	Butyl	A,B	12.99
M11	BPR28	Butyl	B	3.18
M12	BPR35	Butyl	B	6.13
M13	BPR46	Butyl	B	31.23
M14	BPR62	Butyl	A,B	-[a]
M15	BPR76	Ethyl	B	-[a]

[a] impurities impeded the purification; [b] abbreviation according to the lab book.

4.1.1 Monomer Synthesis Method A

N-Methyl and *N*-butyl are denoted with R, since the synthesis of the monomers follows the same procedure, exceptions will be described. The synthesis of R-NCA according to method A is based on the protocol of *Luxenhofer et. al.* [27] with minor adjustments. Due to the purchase of sarcosine the synthesis of R_1-A1 and R_1-B2 was spared.

Synthesis *N*-R-glycine Hydrochloride (R-A1)

Glyoxylic acid (GA) monohydrate, R-amine and CH_2Cl_2 were mixed together and stirred at room temperature for 24 hours, the solution turned turbid white after 2 hours. After 24 hours the solvent was evaporated and the solution was acidified. The mixture was heated under reflux for further 24 hours (Figure 20). White crystals were obtained after evaporation of the solvent. The solid was dissolved in a small amount of methanol, slightly heated with the heat gun if necessary, and precipitated with diethyl ether (R_2-B1: 59.5 %).

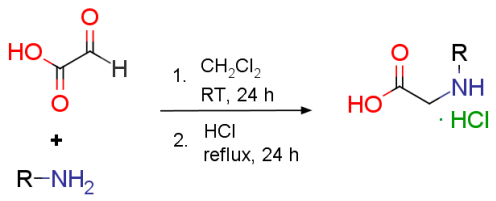

Figure 20: Leuckart-Wallach reaction between glyoxylic acid and amine.

Synthesis of *N*-Benzyloxycarbonyl-*N*-R-glycine (R-A2)

R-A1 was suspended in toluene and cooled down to 0 °C in an ice bath. Sodium hydroxide, dissolved in Milli Q water, was added to the cooled suspension, yielding a two phase system. Benzyl chloroformate was slowly added to the mixture and the ice bath was removed, preventing the suspension to freeze (Figure 21). The reaction mixture was stirred for 4 hours. It should be noted, that the mixing speed is high enough to allow both phases to interact with each other – this is crucial when it comes to bigger reaction volumes. After that the phases got separated, the aqueous layer was returned to the flask and its pH value was reduced to 1 with HCl. The acidified solution was extracted with ethyl acetate, the resulting organic phase was washed with brine, dried over magnesium sulfate, filtered and dried under reduced pressure yielding a yellowish oil (R_1-A2: 92.7 %, R_2-A2: 70.9 %).

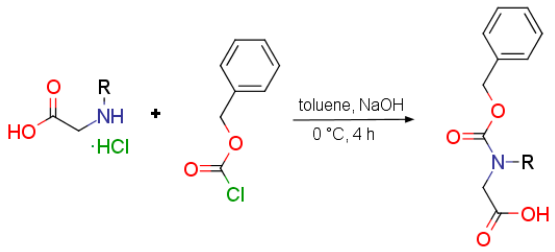

Figure 21: Condensation of R-A1 with benzyl chloroformate resulting in a carbamate.

Synthesis of *N*-R-*N*-carboxyanhydride

Dry acetyl chloride and acetic anhydride were added to the yellowish oil (R-A2) under N_2 atmosphere. This step was carried out in a two- or three-necked-flask with a constant N_2 flow to guarantee inert conditions, schematically shown in Figure 22.

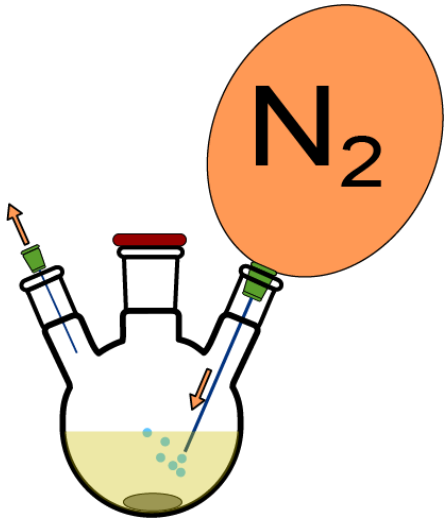

Figure 22: Three-necked-flask, half filled with reaction mixture and a magnetic stirrer on the bottom. All necks are closed with septums. The balloon, filled with N_2, on the right side guarantees inert atmosphere, when the N_2 flow can pass through an outlet needle (left neck). Reagents can be added via the middle neck.

The reaction mixture was heated under reflux. The condenser was flushed with nitrogen to prevent the reaction to get in contact with water molecules. Followed by evaporation of acetyl chloride and acetic anhydride, yielding in a brownish solid (Me-NCA) or crude oil (Bu-NCA).

Once the ring closure is accomplished every further working step has to be carried out under inert atmosphere to prevent polymerization. The flask with the crude product was transferred into the glovebox. In the case of Me-NCA the content was scraped out into a sublimation device. The sublimation device got channeled out of the glovebox and was connected to an ultra-high vacuum pump. Many attempts were undertaken to purify Me-NCA synthesized by method A, but acetic anhydride could not be evaporated completely and residues were still in the crude

product. This impurity prevented the pure Me-NCA crystals from sticking to the cooling finger and caused re-mixing with the unpurified product.

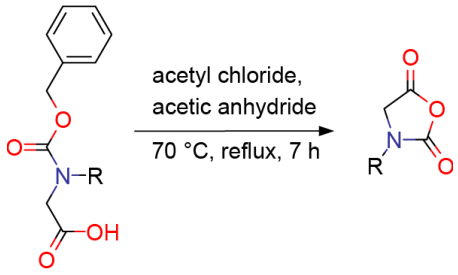

Figure 23: Ring closure of *N*-carboxy anhydride by ring closure under acidic conditions.

In the case of Bu-NCA the crude oil was purified by distillation, but residues of the solvent hampered the purification, only impure Bu-NCA (yield: 35%) could be obtained. The combination of Bu-NCA and acetic anhydride led to an azeotropic mixture, which is not possible to separate by distillation. Due to the purification problem, further NCA syntheses were carried out with method B.

4.1.2 Monomer Synthesis Method B

The synthesis of Me-NCA according to method B is based on the protocol of *Zhang et al.* [36] with minor adjustments.

Synthesis of (S)-Methyl 2-(1-R-amino)acetate (R-B1)

N-R-amine, triethylamine (Et_3N) and methyl bromacetate were added to ethyl acetate in round flask at room temperature (Figure 24). The solution turned cloudy and was mixed 16 hours at 55 °C. Milli Q was added, after the mixture was cooled down to room temperature. The aqueous phase was discarded and the organic phase was washed with brine, dried over magnesium sulfate, filtered, the organic solvent was evaporated and yielded in a slightly yellowish clear oil (R_2-B1: 97.5%).

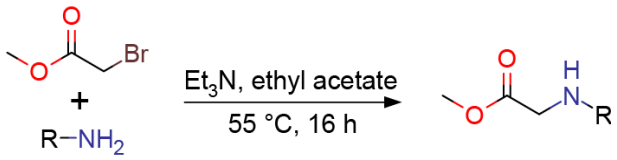

Figure 24: Alkylation of R-amine with bromacetate.

Synthesis of (S)-2-1-(1-R-amino)acetic acid hydrochloride (R-B2)

R-B1 was dissolved in an HCl solution and the pH was controlled with pH paper (Figure 25). Additional HCl was added till a pH range 1-2 was obtained. The reaction mixture was stirred for 16 hours at 55 °C. The solvent was removed under vacuum, yellow-white crystals were obtained (R_2-B2: 94.9%)

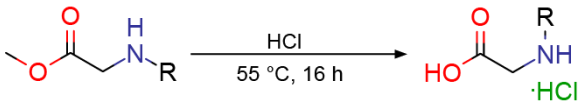

Figure 25: Hydrolysis of ester with HCl.

Synthesis of (S)-2-[tert-butoxycarbonyl-R-amino]acetic acid (R-B3)

R-B1, Milli Q water, triethylamine and di-tert-butyl dicarbonate (Boc_2O) were filled into a flask. The reaction mixture was stirred for 16 hours at room temperature and extracted with hexane. The aqueous phase was poured slowly into an aqueous HCl solution (Figure 26). According to *Luxenhofer et. al.* [27] this acidification should be enough, but it has proven that a pH adjustment in range of pH 1-2 with aqueous HCl results in a better yield. The mixture was extracted with ethyl acetate, washed with brine, dried over magnesium sulfate and filtered. The solvent was evaporated under vacuum and afforded a bluish (R_1-B3: 90.2 %) or yellowish oil (R_2-B3: 81.4 %).

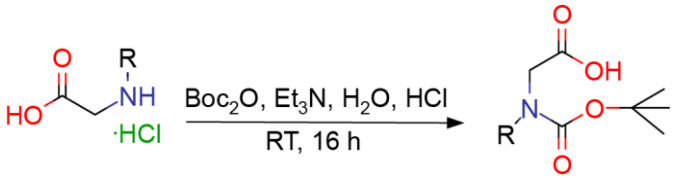

Figure 26: Protection of the amine group with Boc_2O.

Synthesis of *N*-R-*N*-carboxyanhydride

The same reaction construction as seen in Figure 22 was used for this step. R-B3 was dissolved in anhydrous dichlormethane (CH_2Cl_2) in a three-necked-flask under nitrogen, cooled down to 0°C with an ice batch and PCl_3 was slowly added (Figure 27).

A yellowish-brownish solid was obtained after inert evaporation of the solvent. Then the flask was channeled into the glovebox, resuspended with dry CH_2Cl_2 and sodium hydride (NaH) was added to eliminate PCl_3 residues. This mixture was once stirred for 16 hours (M5) and once only 30 minutes (M7). The longer mixing duration did not enhance the yield. Next the suspension was filtered, transferred out of the glovebox and the solvent was evaporated.

Once more the flask was brought back into glovebox. In the case of Me-NCA the solid product was scraped out into the sublimation device followed by sublimation at the high vacuum pump outside the box. Before heating up the device, high vacuum was applied for 2 hours to evaporate the remaining solvent. In the case of Bu-NCA purification process was done by distillation. The best results for pure Bu-NCA were obtained by distillation at 110 °C and 0.04 mbar (M13). Furthermore in the first attempts to purify the NCA, the chosen distillation device was over sized, where only little to no yield was achieved. Since Bu-NCA has a high viscosity it is recommended to not let the parts of the distillation device to cool out. Heating the parts with the heat gun can provide remedy.

Working with Boc_2O as protective group for the amine was much better than using acetyl chloride and anhydride as solvent. With method B Me-NCA yielded in white crystals with no further purification problems.

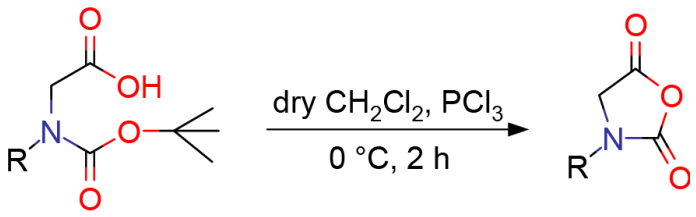

Figure 27: *N*-carboxy anhydrides by ring closure of R-B3 with PCl_3.

4.1.3 Monomer Synthesis of *N*-Butyl-*N*-Carboxyanhydride Method A & B

Since method A & B are partially overlapping, they can be combined, which was tried twice (M10, M14). The first synthesis step was done according to method A (R_2-A1) and as protective group Boc_2O was used (R_2-B2, R_2-B3). This combination showed no significant yield improvement to method B, but purification was easier than with method A.

4.1.4 Monomer Synthesis of *N*-Ethyl-*N*-Carboxyanhydride Method B

In contrast to Me- and Bu-NCA syntheses, only method B was used for synthesis of Et-NCA, since method B has been proved to be more successful when it comes to purification. However, Et-NCA was not successfully synthesized in the course of this thesis.

The synthesis pathway is very similar as described in detail in chapter 4.1.2, only deviations from the protocol of *Zhang et al.* [36] will be discussed in detail in the following chapters.

Synthesis of (S)-Methyl 2-(1-ethylamino)acetate (R_3-B1)

N-ethylamine in THF served as starting material and the stirring duration was expanded to 30 hours. White crystals were obtained (yield: 64.3 %).

Synthesis of (S)-2-1-(1-ethylamino)acetic acid hydrochloride (R_3-B2)

After mixing HCl together with R_3-B1 the solution turned orange to brownish. The evaporation of the solvent yielded in a red/orange colored oil. At this step the product should be recrystallized, but recrystallization with MeOH/THF 0 °C yielded in no crystals. Therefore the solution was stored at -20 °C for 16 hours to enhance crystallization. This temperature change made the product more viscous than the solvent and could be separated. Evaporation of the remaining solvent yielded in white to slightly orange crystals (yield: 50.3 %).

Synthesis of (S)-2-[tert-butoxycarbonyl-ethylamino]acetic acid (R_3-B3)

Due to the insufficient recrystallization process of R_3-B2 only a fraction of R_3-B2 was processed with Boc_2O. A yellowish oil was obtained (yield: 21.8 %).

Synthesis of *N*-Ethyl-N-carboxyanhydride

Owing to the low yield of R_3-B3, several batches of R_3-B3 were mixed together to have enough material for distillation.

Et-NCA could not be successfully purified by distillation. The viscosity of the product was too high which made it impossible to distill it with our equipment. The device was heated up to 160 °C, the reduced vacuum was at 0.04 mbar and the distillation parts were kept hot with the heat gun, but still no product was obtained.

4.1.5 Overall Discussion of Monomer Synthesis

Based on the carried out syntheses and their success or failure, method B has proved to be the better option for Me- or Bu-NCA synthesis. The solvent used in method A made it impossible to purify the crude product. The possibility to evaporate solvent inside the glovebox and working with a schlenkline could enhance the yield of the product.

4.2 Polymer Synthesis

In this thesis we put our focus on six different compositions of polypeptoids, which were further investigated in their LCST, kinetics and molecular weight.

Table 2: Copolymerization of Me-NCA with Bu-NCA initiated by nitrodopamine-modified SPION.

Abbr.	Me-NCA [a] [%]	Me-NCA [b] [%]	Mn[c] [g/mol]	T_{CP}[a]	T_{CP}[d]	PDI[c]	σ [M/nm^2]	D_H [nm][d]
P1	46.00	60.7	2106	27	33 °C	1.06	1.5	13.3 ± 1.5
P2	50.24	65.8	2454	37	47 °C	1.10	1.8	13.2 ± 1.4
P3	51.05	64.6	2372	40	44 °C	1.09	2.2	10.8 ± 0.7
P4	58.00	68.7	2400	47	41 °C	1.12	2.0	12.5 ± 1.4
P5	55.26	73.5	2544	54	-[e]	1.09	1.4	9.1 ± 0.5
P6	56.05	72.6	2325	62	58 °C	1.13	1.8	11.9 ± 1.0

All polymerization were calculated on final molecular weight of 20000 g/mol. [a] as calculated according to literature [45]. [b] as calculated by H^1 NMR analyses. [c] as determined by MALDI-TOF MS. [d] as determined by DLS. [e] unable to measure. All polymerizations were initiated with nitrodopamine-modified SPIONs (6.5 ± 0.6 nm).

The calculation for the desired LCST value (Table 2) was based on the work of *Ling et. al.* They investigated co-polypeptoids synthesized by copolymerization of Sarcosine *N*-thiocarboxyanhydrides and *N*-butylglycine *N*-thiocarboxyanhydrides. Their research results revealed that high molecular weight and low Sarcosine molar fraction of the copolymer lowers the LCST [45]. For polymerization of our polypeptoids six different ratios of Me- and Bu-NCAs were used. As initiator nitrodopamine as ligand on SPIONs. The core particles were single-crystal, monodisperse with a diameter of 6.5 ± 0.6 nm (Figure 28).

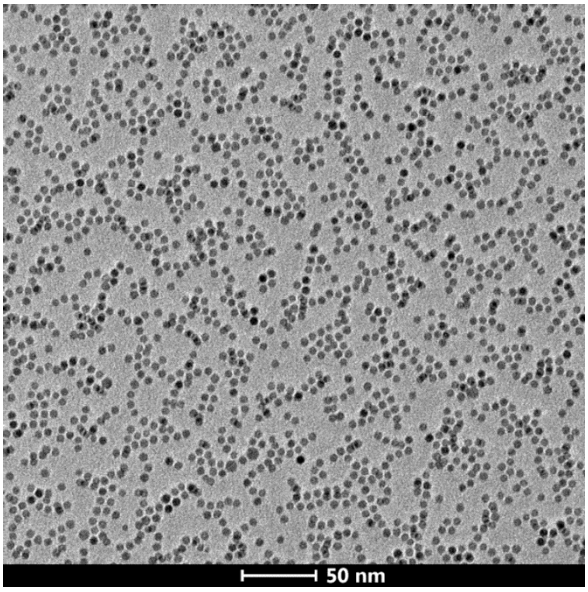

Figure 28: TEM picture showing single-crystal, monodisperse Fe_3O_4 particles with oleic acid as ligand.

4.2.1 Prerequisites and Optimization of Polymerization Conditions

Before using SPIONs as initiator for polymerization the amount of bound nitrodopamine, after the ligand exchange, has to be analyzed by TGA. With the number of bound nitrodopamine the amount of SPIONs needed for polymerization can be calculated. According to TGA the used Fe_3O_4 cores correspond to 8.9 molecules per nm². However, the theoretically maximal grafting density of nitrodopamine on SPIONs is around 3 molecules per nm² per molecule [15],[46]. This result showed, that even after several washing steps during purification, SPIONs were still surrounded by free nitrodopamine. It is possible that residues of OA are responsible for the high grafting density as well, but OA residues should not be problematic for polymerization on the trace level, since OA does not quench the polypeptoid synthesis. Despite of using different purification methods such as dialysis and using different wash protocols, no improvement of purity was possible. The excess of free nitrodopamine was taken into account, when calculating the molecular weight of the polymer.

A further requirement to obtain homogeneous polymerization on all NPs is to find conditions, where nitrodopamine-modified SPION and already polymer-modified SPION are both completely dispersed. This prerequisite implies a need for a solvent, where all components are soluble. A wide range of organic solvents (*N*, *N*-dimethyl acetamide, *N*, *N*-dimethylformamide, sulfolane, tetramethyl urea, toluene and THF) were tested. The monomers and NP were soluble in THF but yielded in agglomerates and clusters when polymerized (Figure 29 A-C).

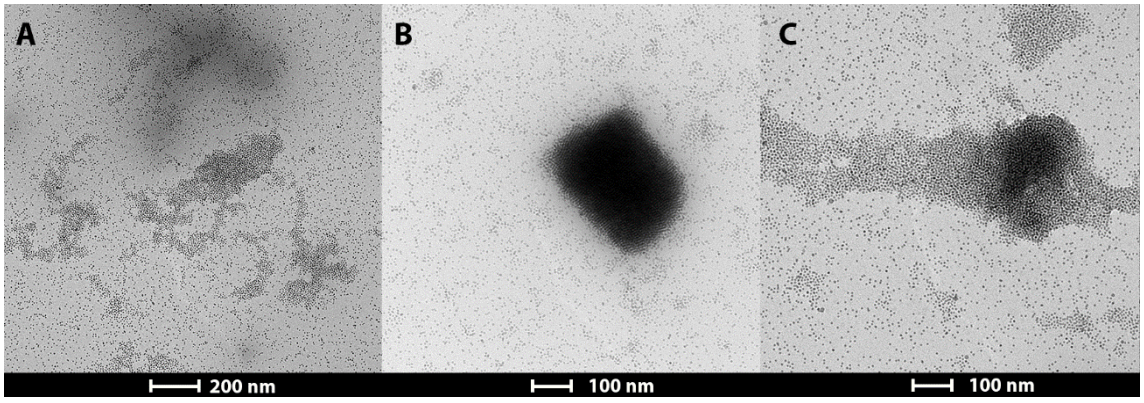

Figure 29: TEM picture of SPION clusters obtained after surface initiated polymerization in THF.

DLS measurements confirmed the agglomeration of CSNP when polymerized in THF, yielding an average hydrodynamic diameter of 102 nm (Figure 30).

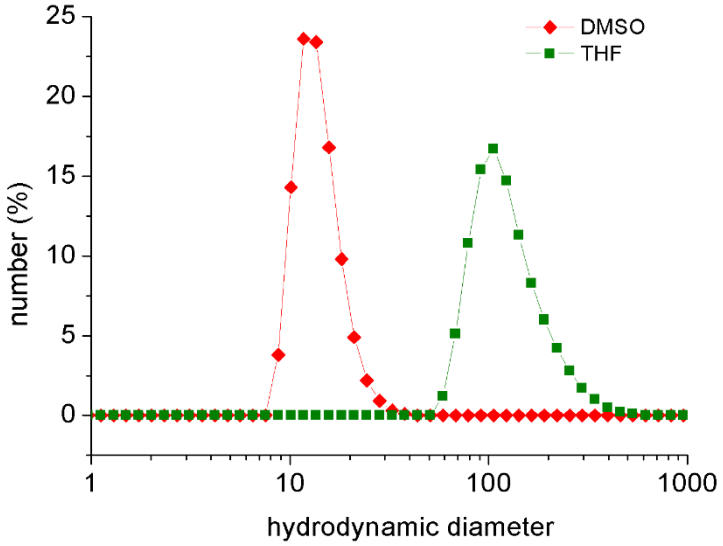

Figure 30: Comparison of the hydrodynamic diameter of P1 CSNP polymerized in DMSO and THF (number weighted distribution).

Only DMSO met the required conditions and resulted in completely dispersed nitrodopamine-coated SPION. Unfortunately there is evidence that DMSO causes spontaneous polymerization which leads to cyclic polypeptoid (macrocycle) formation [47]. *Zhang et. al.* assumes that not DMSO itself but nucleophilic impurities in the solvent are responsible for solvent-induced polymerization [48]. This predicament makes it difficult to purchase a solvent in the desired quality, since commercial anhydrous DMSO might include nucleophilic impurities. In spite of possible side reactions DMSO ensured well dispersed SPION, while other solvents (e.g. THF) led to aggregate formation (Figure 29). Nitrodropamine hydrogensulfate was converted to its neutral amine-form with *N*-methylpyrrolidone (NMP), which is essential for starting the polymerization.

4.2.2 Kinetic Investigation of Polypeptoid-Modified SPION

The procedure of synthesizing the polymer was always kept the same and was carried out in a GS glovebox. The glass vial was loaded with the solvent, NMP and a magnetic bean. Next Bu- and Me-NCA were added to the reaction mixture. The initiator, nitrodopamine-modified SPION, was added to the mixture to start the polymerization. The reaction mixtures were calculated on final molecular weight of 20 kDa. All reactions were carried out at 22 and 50 °C.

A kinetic study, analyzed with MALDI-TOF MS, showed clear differences after 24 hours between the temperatures (Figure 31 & Figure 32). Two identical CSNP polymerization were carried out, once at 22 °C and once at 50 °C. Samples were taken and analyzed after 2, 6, 24 and 72 hours.

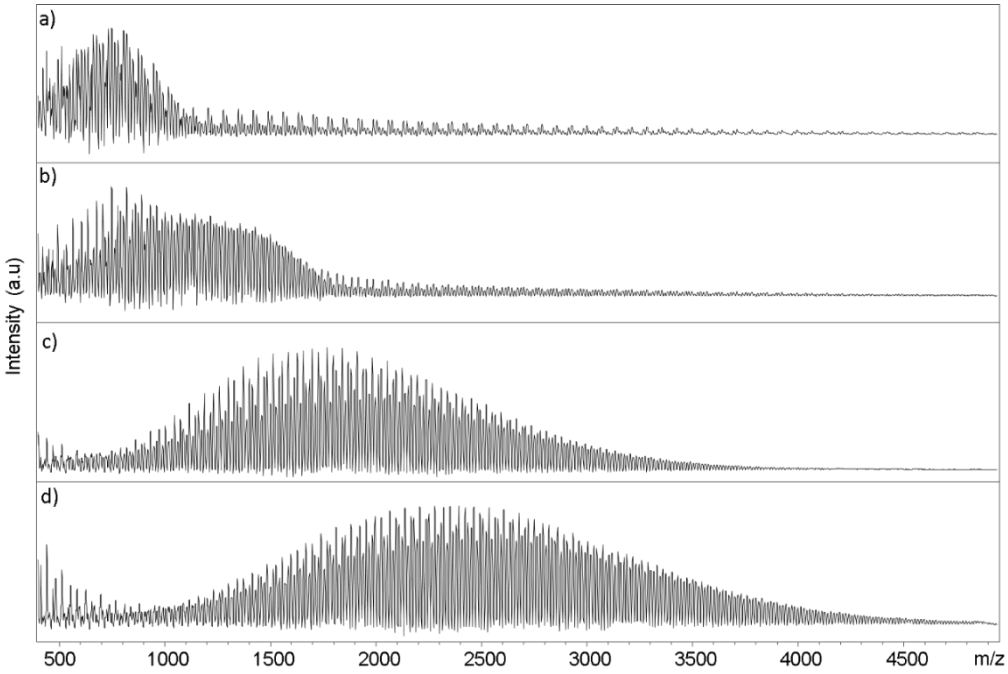

Figure 31: MALDI-TOF mass spectra of surface initiated co-polymerization of Me-NCA and Bu-NCA in DMSO at 22°C after 2 h (a), 6 h (b), 24 h (c) and 72 h (d)

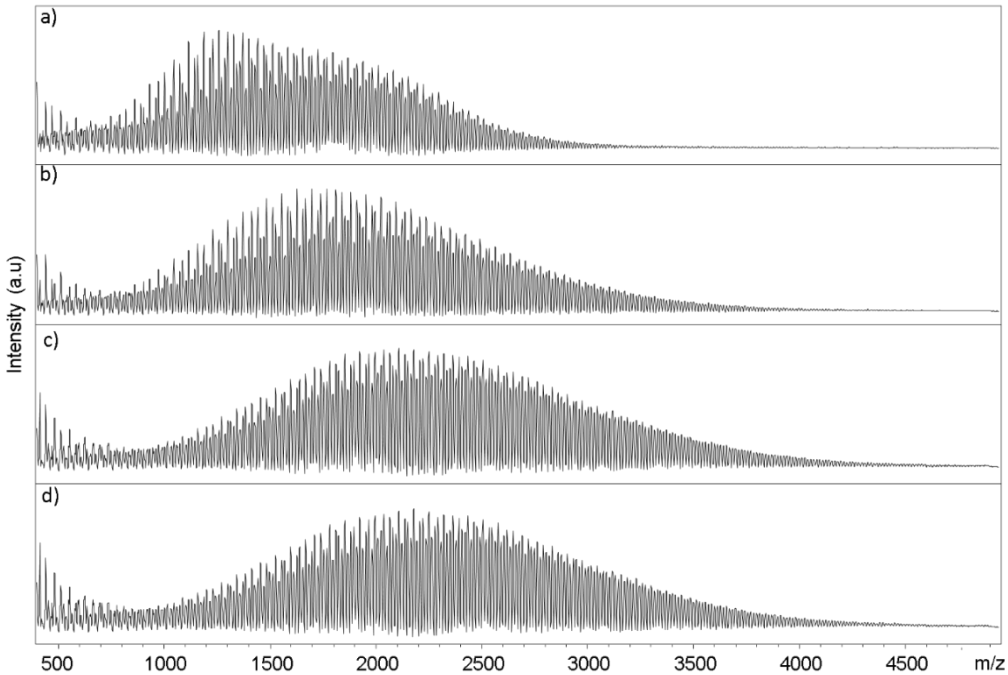

Figure 32: MALDI-TOF mass spectra of surface initiated co-polymerization of Me-NCA and Bu-NCA in DMSO at 50°C after 2 h (a), 6 h (b), 24 h (c) and 72 h (d).

It was expected that higher temperature causes higher molecular diffusion, leading to faster polymerization. Although it was not certain, if higher temperature harms the MW or PDI of the polymer due to thermal initiated free polymerization. MALDI-TOF MS show, as seen in Figure 33, that the PDI and final molecular weight of both reactions are comparable, despite the temperature difference. However, polymerization at 50 °C reaches the final molecular weight of 2.1 kDa after 24 hours with no further increase after 72 hours, whereby polymerization at 22 °C is slower and reaches the final molecular weight after 72 hours. All further polymerizations were carried out at 50 °C.

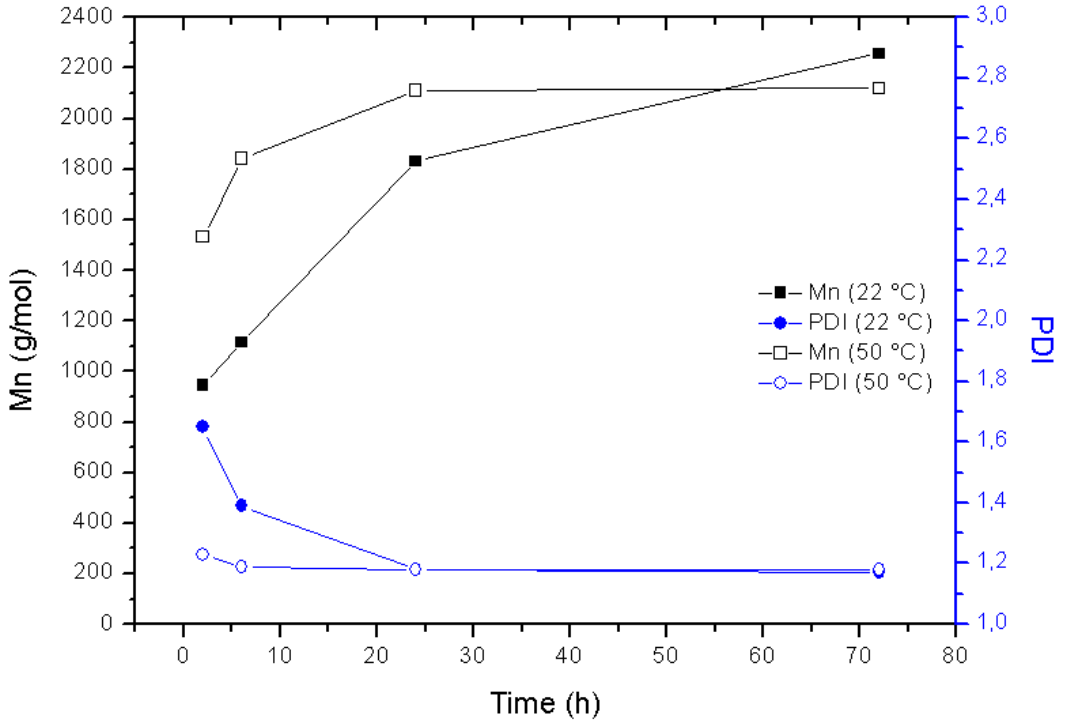

Figure 33: Evolution of number average molecular weight and polydispersity (measured by MALDI-TOF MS) for surface-initiated co-polymerization of Me-NCA and Bu-NCA in DMSO at 22 and 50 °C.

It was tried to evaluate the molecular weight of the polypeptoid with GPC as an alternative method to MALDI-TOF. It was expected to identify a spectra with single peaks, but GPC investigations led to dimeric peaks where the mass peak of the sample was overlapping with the artefact peak of the instrument. It was not possible to characterize the polypeptoids with our existing system. To make the characterization of the polypeptoids feasible with GPC a different column with a higher resolution in the low molecular weight range and optimization of the mobile phase is needed to suppress dimerization of the peaks.

4.2.3 Molecular Weight Analysis of Polypeptoid-Modified SPION

Sample P1-P6, polymerized from SPION, were analyzed by MALDI-TOF MS. The mass spectra show a polymer distribution from 400 to 4000 m/z (Figure 34). Peaks in the range from 400 to 1000 m/z can be assigned to macrocyclic structures. The main polymer distribution ranges from 1000 to 4000 m/z and can be assigned to lithium-doped, nitrodopamine-initiated co-polymer chains with protonated terminal group (Figure 35).

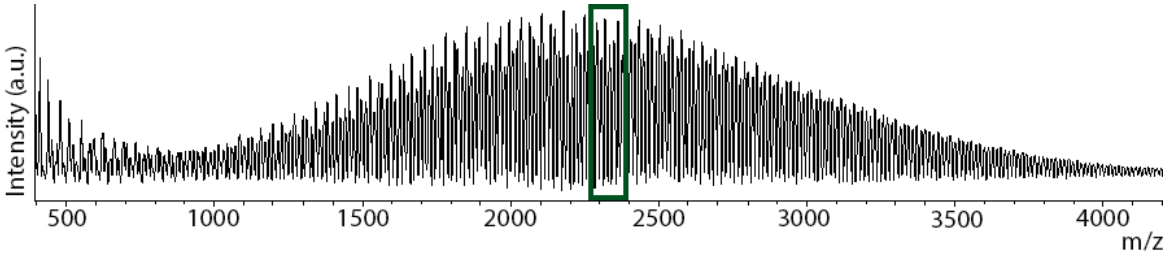

Figure 34: Full MALDI-TOF mass spectrum of sample P2 after 24 hours, DHB, LiTFA, linear positive mode.

The MALDI-TOF MS spectra show molecular weights between 2.1 – 2.5 kDa (Table 2) and are lower than calculated. The small size of the polymer is attributed to the solvent-induced initiation by DMSO and/or nucleophilic impurities generating macrocycles [47] as side products. However, the narrow polydispersities in the range of 1.06 to 1.13 indicate controlled polymerization.

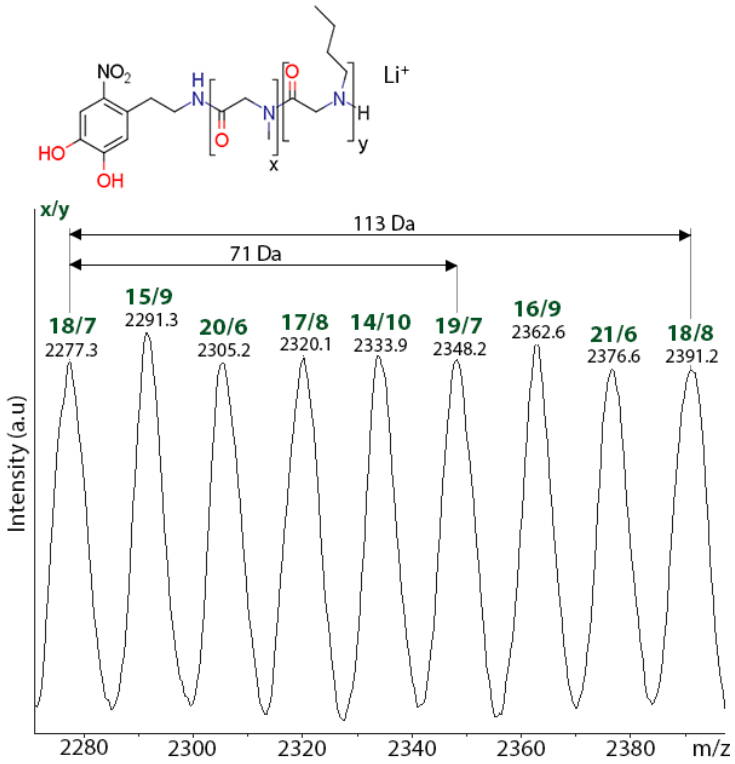

Figure 35: MALDI-TOF mass spectrum of sample P1 (DHB, LiTFA, linear positive mode), enlargement from 2270 to 2400 m/z, protonated copolymer species of the given formula with x/y: ratio of *N*-methylglycine / *N*-butylglycine units (green labels).

The information about m/z of every peak allows to assign every signal to a ratio of *N*-methylglycine / *N*-butylglycine unit (Table 3) confirming that the investigated polymer is the desired co-polypeptoid.

Table 3: MALDI-TOF MS peak calculation of sample P1.

m/z experiment	m/z calculated	x^a	y^b
2277.3	2276.6	18	7
2291.3	2289.7	15	9
2305.2	2305.6	20	6
2320.1	2318.7	17	8
2333.9	2331.8	14	10
2348.2	2347.7	19	7
2362.6	2360.8	16	9
2376.6	2376.7	21	6
2391.2	2389.8	18	8

Calc. with Isotope Pattern Analysis (Bruker Daltonics); [a] number of *N*-methylglycine , [b] *N*-butylglycine units.

In order to determine the development of the molecular weight with repeated monomer addition a kinetic study was carried out and analyzed with MALDI-TOF MS (Figure 36). It was expected that the molecular weight increases infinitely as long as fresh monomer is added, since this polymerization has a "living polymerization character". The secondary amine as end-group of the growing polymer should make further chain extension possible.

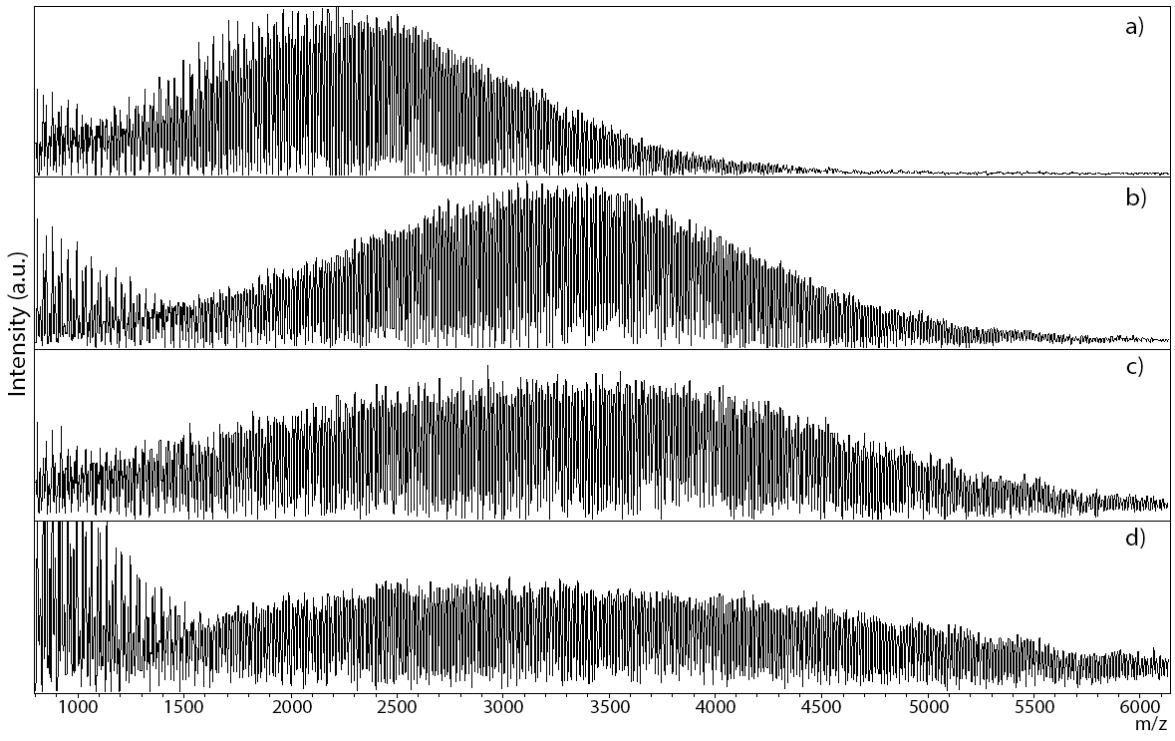

Figure 36: MALDI-TOF mass spectra of surface initiated co-polymerization of Me-NCA and Bu-NCA in DMSO at 50°C; a) after 24 h, b) 48 h (after 1st addition), c) 72 h (after 2nd addition), d) 96 h (after 3rd addition).

Table 4: Results of step-wise monomer addition experiment.

Sample	reaction time [h]	Mn [g/mol]	PDI
Copolymer	24	2338	1.21
1st addition	48	3008	1.17
2nd addition	72	3032	1.22
3rd addition	96	2982	1.32

The MALDI-TOF MS measurements show that the increase of the average molecular weight stops after 48 hours (Figure 36 b, Figure 37). The PDI tends to get higher over time, indicating that the control of polymerization is lost. Especially notable is the high intensity of polymer ranging from 0 to 1600 m/z (Figure 36 d), which shows that fresh monomer started to form macrocycle structures. The macrocycle formation was confirmed by peak analysis (Figure 38) of the MALDI-TOF MS spectra seen in Figure 36 d.

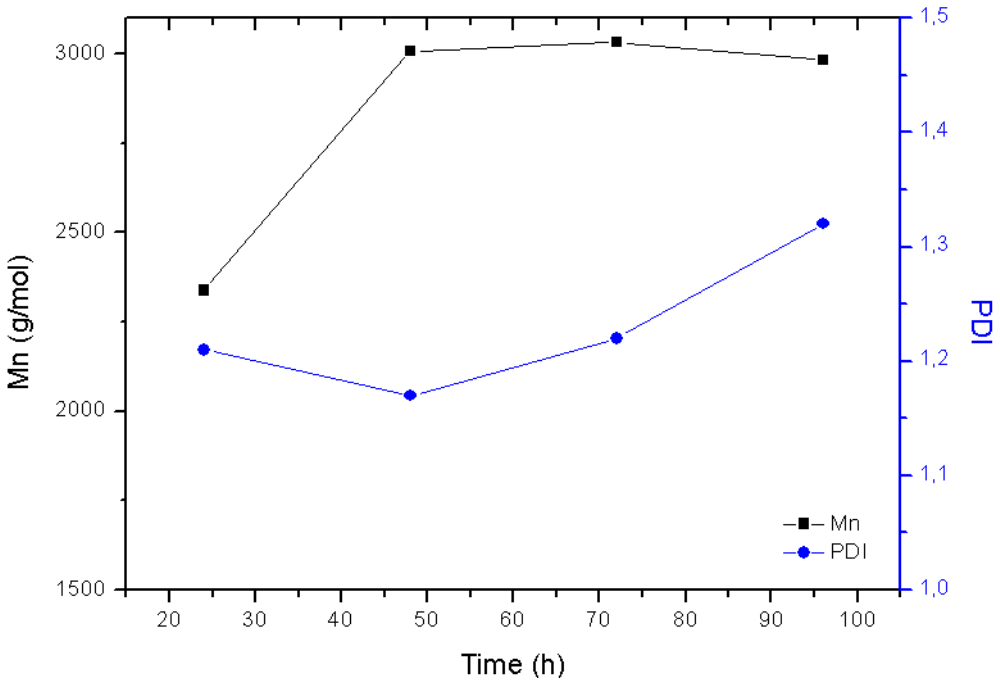

Figure 37: Evolution of number average molecular weight and polydispersity (measured by MALDI-TOF MS) for step-wise monomer addition experiment (surface-initiated co-polymerization).

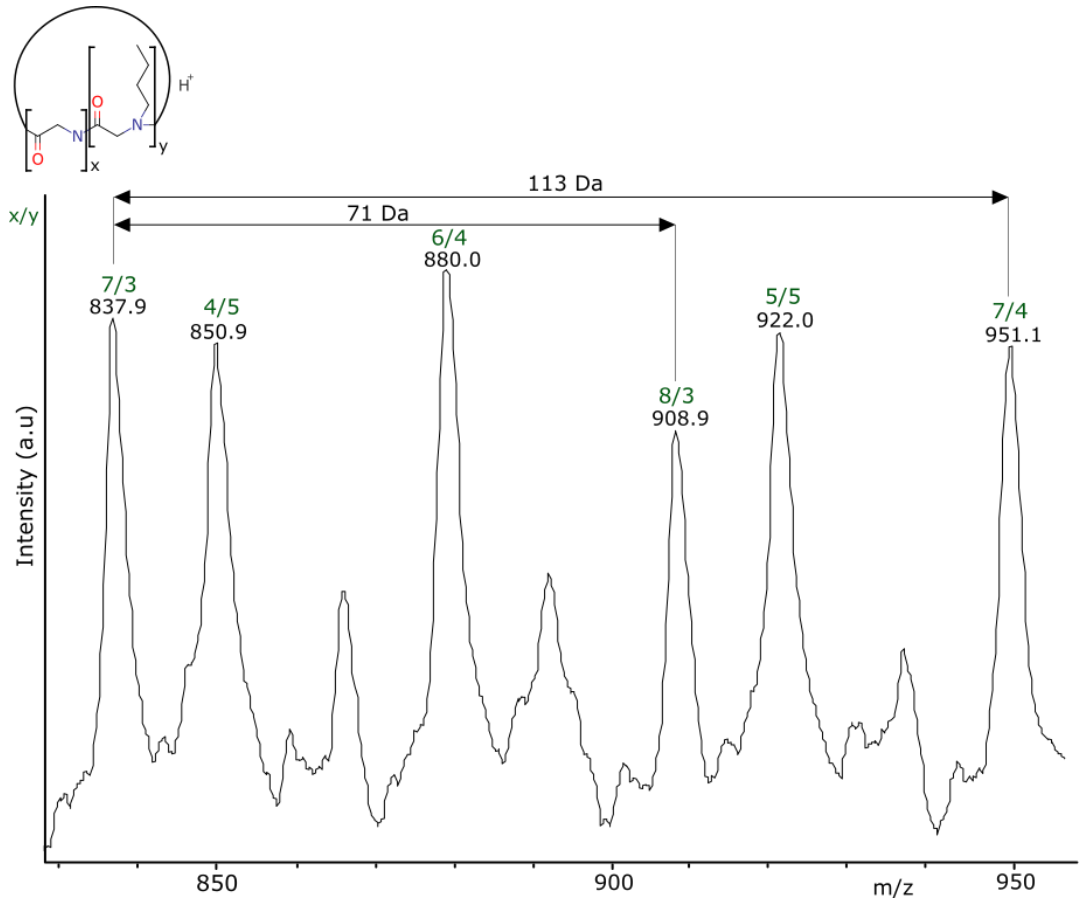

Figure 38: MALDI-TOF mass spectrum of macrocycle section (DHB, LiTFA, linear positive mode), enlargement from 830 to 960 m/z, protonated copolymer species of the given formula with x/y: ratio of *N*-methylglycine / *N*-butylglycine units (green labels). The unassigned peaks result from matrix noises.

Table 5 MALDI-TOF MS peak calculation of macrocycle section of step-wise addition experiment.

m/z experiment	m/z calculated	x^a	y^b
837.9	838.0	7	3
850.9	851.1	4	5
880.0	880.1	6	4
908.9	909.1	8	3
922.0	922.2	5	5
951.1	951.2	7	4

Calc. with Isotope Pattern Analysis (Bruker Daltonics); [a] number of *N*-methylglycine , [b] *N*-butylglycine units.

It can be assumed that impurities in the solvent or DMSO in general is responsible for the low yield in molecular weight and forming macrocycles.

4.2.4 Composition Analysis of the Polypeptoid Shell

The composition of the co-polymer was determined by ^{1}H-NMR (Figure 39). Raw polymer-modified SPION were dissolved in HCl and purified by dialysis (MWCO: 500 Da).

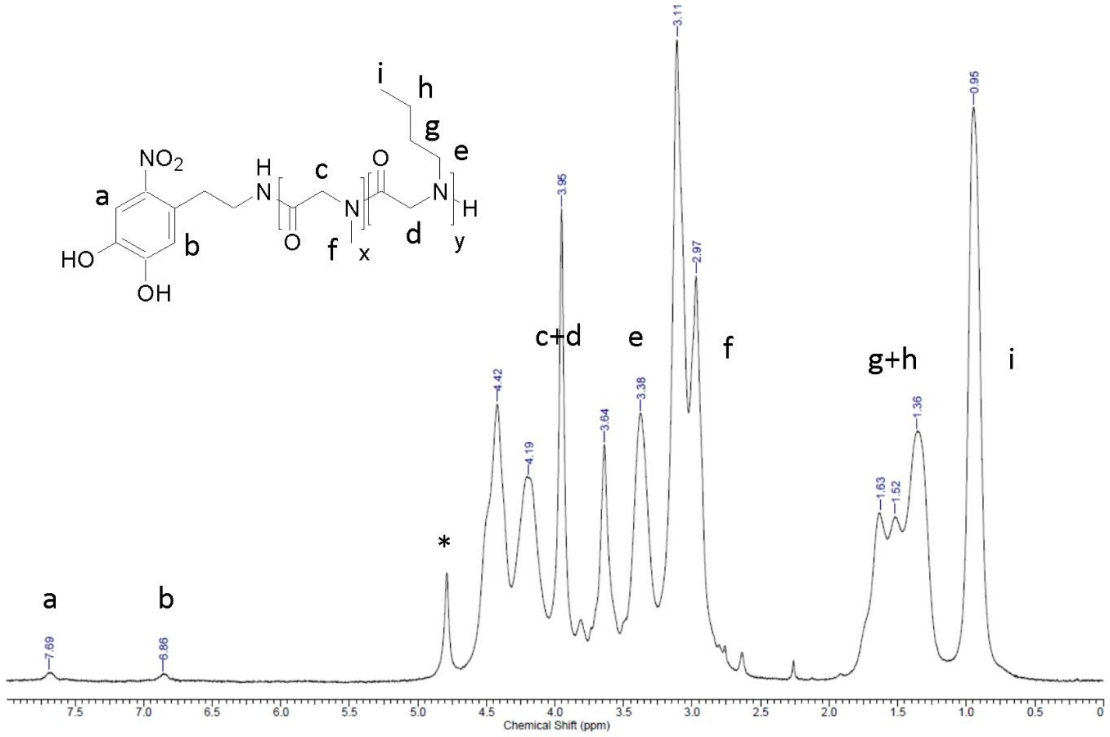

Figure 39: ^{1}H-NMR spectrum of isolated polymer shell of sample P1 in D_2O, * solvent peak.

Nitrocatechol end-group peaks at 7.69 and 6.85 ppm prove the initiation by nitrodopamine. With the relationship between peak i and e+f the fraction of *N*-methylglycine units can be calculated. There is a recognisable trend for a higher fraction of *N*-methylglycine in the polymer composition. The actual *N*-methylglycine ratio is on average 28.41% higher than the calculated proportion (Table 2), indicating a higher reactivity of Me-NCA compared Bu-NCA. This trend was already reported in literature [27].

4.2.5 Grafting Density Investigation of the Polypeptoid-Modified SPION

To determine the grafting density and the size distribution of the CSNP, the raw particles have to be purified. The removal of excess of free polymer is necessary to obtain accurate results. The samples were dialyzed for 24 hours (MWCO: 100 kDa), whereby the samples were measured by TGA prior and after purification to determine the reduction in organic mass fraction (Table 2). Flat surfaces modified with surface grafted, done by grafting-to method, polysarcosine show a grafting density up to 0.95 chains nm^{-2}, whereby the investigated CSNP correspond to a grafting density of 1.4 – 2.2 chains nm^{-2} [30]. Figure 40 shows an example of

a TGA evaluation of sample P6 and emphasizes the need for sample purification to remove free polymer.

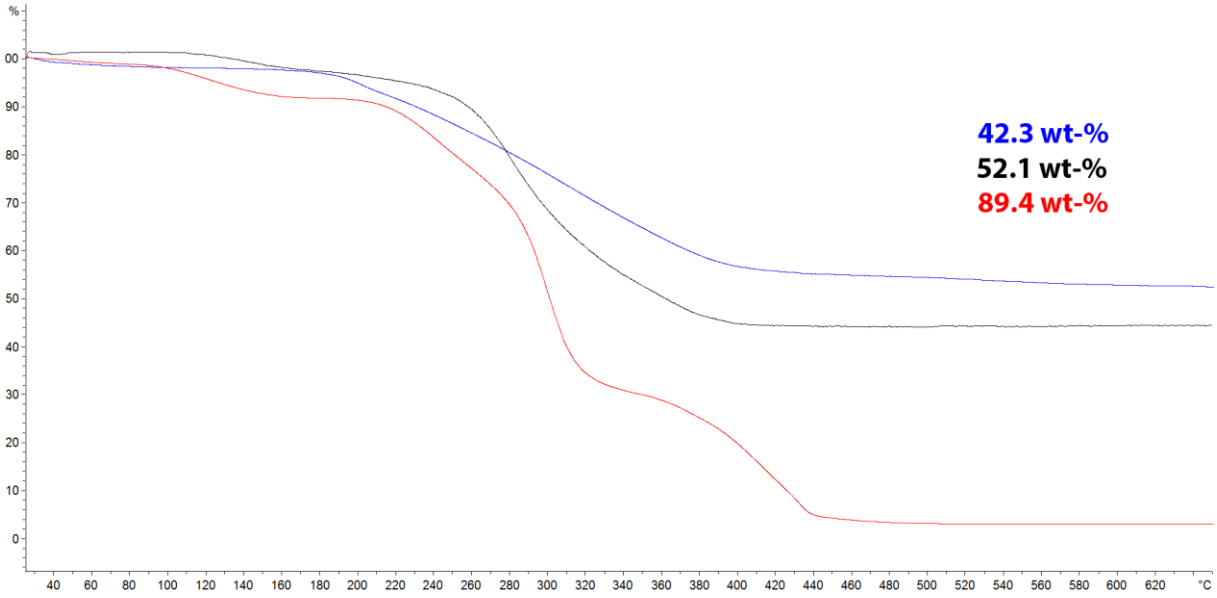

Figure 40: TGA thermograms (25-650 °C, 10 K min^{-1}), blue curve: nitrodopamine coated SPION FeOx-NH_2, red curve: P6 polypeptoid-grafted SPION (raw product), black curve: P6 polypeptoid-grafted SPION (purified).

The hydrodynamic diameter of the CSNP, below the LCST, was determined in Milli Q water by DLS. The expected size was between 9 – 13 nm with a core size of 6.5 nm and a polypeptoid molecular weight between 2.3 – 2.5 kDa. On the basis of the average hydrodynamic diameter of 11.8 nm, the measurements met the expectations. The results show a narrow size distribution ranging from 9.1 to 13.3 nm (Table 2, Figure 41) and stayed constant over weeks in water, indicating an excellent colloidal stability with a polypeptoid shell only 5.3 nm thin.

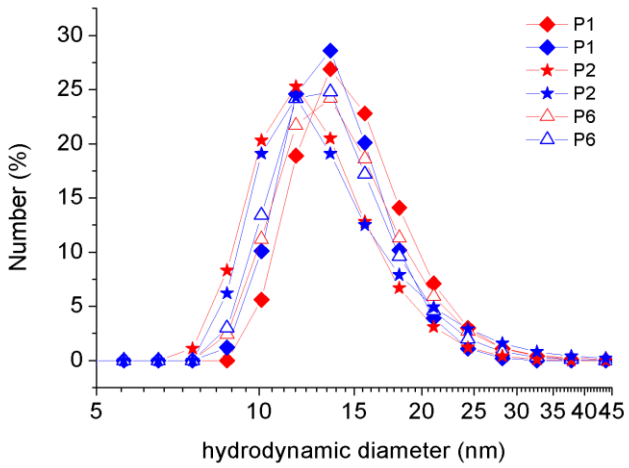

Figure 41: DLS size curves of sample P1, P2 and P6 at 20 °C before and after heating to 70 °C. Red symbols depict the measurements before heating and the blue symbols show the measurements after cooling back to 20 °C.

Mono-dispersity and no cluster-building of aqueous polypeptoid-modified SPION was supported by TEM as well (Figure 42).

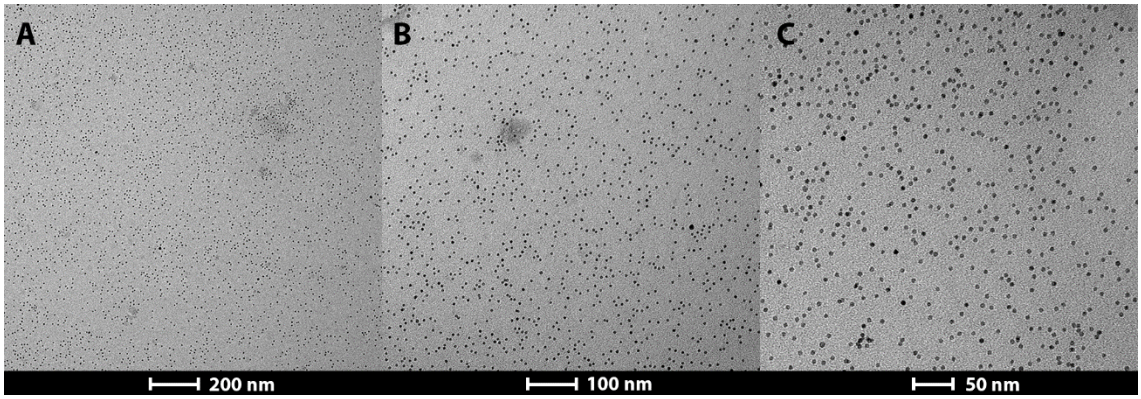

Figure 42: TEM pictures of mono-disperse P1 SPIONs in Milli Q water.

4.2.6 Investigation of Thermoresponsive Properties of the Polypeptoid-Modified SPION

The thermoresponsive properties of the polypeptoid shell were investigated with DLS measurements to assess the LCST of the polymer brush on the SPIONs. Each polypeptoid-grafted SPION sample (P1-P6) was dispersed in Milli Q water to a concentration of 1 mg/ml. The samples were filtered with a 0.45 µm cellulose filter to remove insoluble residues. All samples were heated up from 20 to 70 °C and cooled down back again to 20 °C once and every single temperature step was measured for three times in a row (Figure 43).

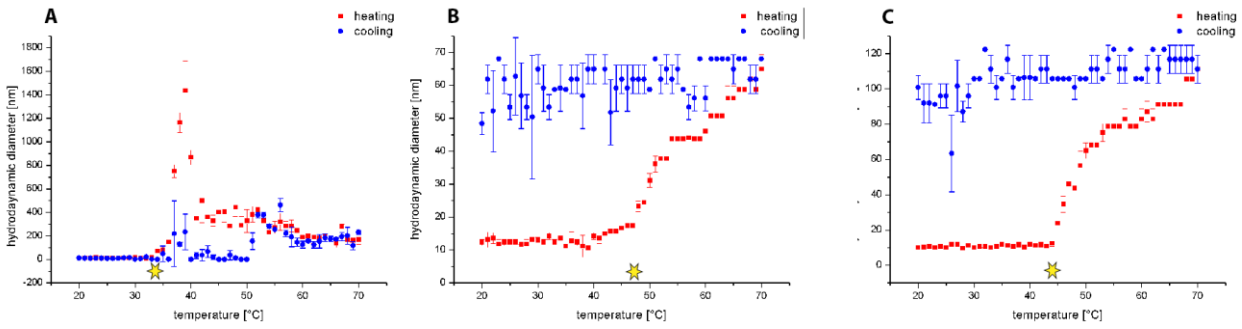

Figure 43: DLS heating and cooling curve of SPION in Milli Q water (1 mg/mL); hydrodynamic diameter vs. temperature; red line with squares shows heating curve; blue line with circles shows cooling curve. (A) for P1, (B) for P2 with hysteresis, (C) for P3 with hysteresis. The yellow star marks the value of the LCST.

For sample P2 and P3 strong hysteresis was observed (Figure 42 B-C). It took the CSNP about 20 hours to return to a dispersed state. This different behavior in agglomeration could not be explained, since the copolymers only differ in their *N*-methylglycine and *N*-butylglycine ratio. The estimated LCST values are based on the average value of the T-cycled measurements. All polymerizations showed increase in size upon heating and returned to the initial value of 12-13 nm when cooling back again. The ability to undergo reversible size change in temperature-cycled measurements show the colloidal stability of the CSNP. The measured LCST (Table 2) are close to the calculated values, but one (P5) value was not measurable. According to literature the LCST gets higher, the higher the *N*-methylglycine unit fraction in the copolymer [45]. Although the *N*-methylglycine and *N*-butylglycine ratio slightly differs from the calculated proportion, this trend was proved as seen in Figure 44. Sample P5 has a molar *N*-methylglycine fraction of 73.5 (Table 2), which is presumable outside the DLS measuring range of 70 °C, supposing it follows the linear trend.

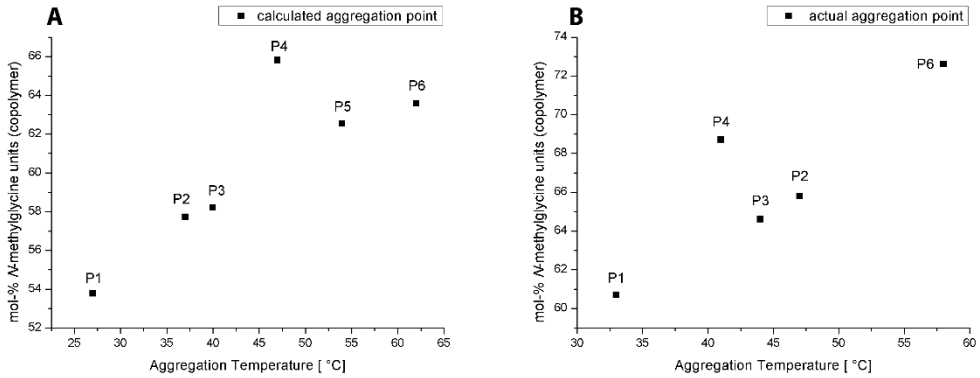

Figure 44: *N*-methylglycine unit fraction plotted against aggregation temperature of copolymer. (A) shows calculated and (B) the measured values.

Colloidal stability of the CSNP was also proved when exposed to a magnetic field. In Milli Q water dispersed P6 polypeptoid-modified SPION (3 mg/mL) did not aggregate when placed in a constant magnetic field at room temperature (Figure 45 A). The solution started to turn turbid at 70 °C, further increase up to 80 °C led to aggregation (Figure 45 B and C). Above the LCST the SPION could be magnetically extracted (Figure 45 C). The precipitated particles could be redispersed after cooling down to room temperature and gentle shaking (Figure 45 D).

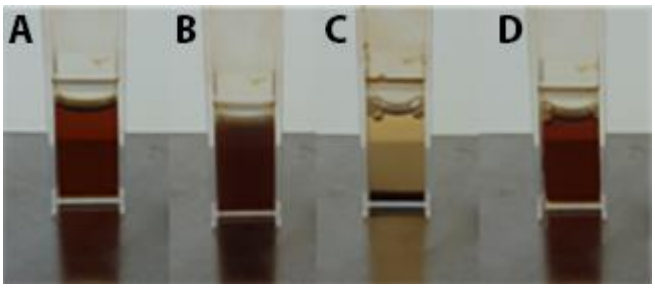

Figure 45: Purified P6-modified SPION dispersion in MilliQ water (3 mg/mL) on a static magnet. (A) at room temperature, (B) heated up to 70 °C, (C) heated up to 80 °C, (D) cooled down to room temperature, gently shaken.

5 CONCLUSION

To conclude, colloidal stable polypeptoid-modified SPION with six different copolymer compositions in varying LCST behavior were successfully produced by the grafting from method. Although synthesis of Me- and Bu-NCA with a high degree of purity was successful, the low yield of the monomers varying between 3 – 44 % could be enhanced by purification inside the glovebox. The actual composition of the polymer was determined by ^{1}H NMR and showed the favored incorporation of Me-NCA, whereby the correlation between rising *N*-methylglycine unit fraction and increase of the LCST was confirmed, this trend was already shown by Zhang using Et-NCA and Bu-NCA as monomers [49]. A polymer molecular weight of 20 kDa was expected, whereby only 2.4[a] kDa was achieved due to lack of sufficient pure solvent: DMSO is the only suitable solvent for polymerization, but induces macrocycle formation which leads to strong reduction of the molecular weight of the polymer [47]. Investigation of other compatible solvents with less drawback or the purification of commercial available solvents could increase the MW of polypeptoids. The obtained LCST of each polypeptoid composition differs from the calculated value by 6 °C[a]. This deviation might be caused by the low MW of the polypeptoids. However, polydispersities in the range of 1.1[a] show controlled polymerization of the polypeptoid. A reaction temperature of 50 °C led to faster polymerization with no indication of increase of the PDI due to thermal polymerization initiation. TGA measurements showed a polymer grafting density of 1.8[a] M/nm^2 on the SPION, which is twice as high as on similar brushes prepared via "grafting-to" on flat surfaces [30]. The CSNP were redispersable after heating above the LCST and precipitating by treatment with a magnet and showed no loss of function even after weeks. The colloidal stability was further confirmed by TEM showing well dispersed polypeptoid-modified SPION. Precise control of the thermoresponsive behavior and the enhancement of the molecular weight has to be investigated to make this system useful for biomedical applications such as magnetic resonance imaging or drug delivery. Optimization of the solvent and deeper investigation of the kinetic of the polymerization would be a big step in the right direction.

[a] values calculated on the average of the six co-polypeptoids in Table 2.

6 EXPERIMENTAL

6.1 Chemicals

All chemicals used for the synthesis, unless otherwise stated, were purchased from Sigma Aldrich and used as received.

6.2 Methods

6.2.1 NMR

^{1}H and ^{13}C-NMR spectra of monomers and polymers were recorded on a BRUKER AV II 600 spectrometer. All NMR measurements were executed by the Department of Chemistry, BOKU. Protonated solvents ($CDCl_3$: 7.26 ppm (^{1}H), 77.0 ppm (^{13}C), D_2O: 4.79 ppm (^{1}H) were used as reference. Copolymer composition was measured for isolated polymer obtained by dissolution of raw SPION. Measurements were analyzed with the software 2D NMR Processor.

6.2.2 TEM

TEM pictures were recorded by Dr. Ronald Zirbs and Martina Schroffenegger, MSc. with a FEI Tecnai G2, with 160 kV acceleration voltage on carbon-coated grids. The size distribution of the NP were calculated with the software Pebbles.

6.2.3 TGA

The percentage of organic material on CSNP was analyzed by TGA on a Mettler Toledo TGA/DSC1, with 80 ml min^{-1} synthetic air as reactive gas, 20 ml min^{-1} nitrogen as protective gas and a heating rate of 10 K min^{-1} from 25 to 650°C. By using such a large temperature span it is possible to distinguish between moisture or solvent residues (up to 200°C), polypeptoid shell (200-500°C) and the inorganic core (above 500°C).

6.2.4 DLS

The hydrodynamic diameter of the CSNP and their LCST value were analyzed by DLS. All samples were diluted in Milli Q water, filtered with a 0.45 µm cellulose filter and underwent temperature cycling experiments from 22 to 70 °C. Every sample was measured on a Malvern Zetasizer Nano-ZS providing information of the mean values and their standard deviation.

6.2.5 MALDI-TOF MS

Molecular weight and PDI of the polypeptoids were analyzed from raw SPION by MALDI-TOF MS. These measurements were done by the Department of Biotechnology (BOKU) on a Bruker Autoflex speed in linear positive mode. Lithium trifluoracetate (LiTFA) was mixed with the samples dissolved in THF and THF-solutions of 2,5-dihydroxybenzoic acid, used as a matrix.

6.3 Monomer Synthesis

6.3.1 *N*-Methyl-*N*-carboxyanhydride Synthesis Method A

Sarcosine (10 g, 112.24 mmol) was dissolved in 155 mL toluene in a round flask. The glassware was put into in ice bath and cooled down to 0 °C. NaOH (13.75 g, 343.76 mmol) was dissolved in 155 mL Milli Q water and added to the mixture. Benzyl chloroformate (18.85 g, 110.73 mmol) was slowly added and the solution was stirred for 4 hours. After that the mixing was stopped, the organic phase was discarded and the aqueous phase was returned to the flask and acidified with 4 M HCl to a pH value of 1. After that the solution was extracted with ethyl acetate (70 mL each) for three times. The organic phase was washed with brine and dried over anhydrous magnesium sulfate. The solvent was removed under reduced pressure yielding a yellowish oil (24.50 g, 110.00 mmol, 98.00 %).

Acetyl chloride (17.60 g, 224.20 mmol) was added to 24.5 g *N*-benzyloxycarbonyl-*N*-methylglycine (110.00 mmol) and dissolved in acetic anhydride (22.50 g, 220.40 mmol) under dry nitrogen atmosphere. The mixture was heated up to 70 °C and refluxed for 6 hours. Solvent and excess of acetyl chloride were removed under reduced pressure under nitrogen atmosphere, yielding a brownish crude product. The product was purified by sublimation at 0.04 mbar at 100 °C (oil bath temperature), yielding yellow-white crystals (4.53 g, 39.36 mmol, 35.78 %).

6.3.2 *N*-Methyl-*N*-carboxyanhydride Synthesis Method B

Sarcosine (5.00 g, 56.12 mmol), Boc_2O (34.00 g, 155.82 mmol), Et_3N (28.30 mL, 279.00 mmol) and 225 mL Milli Q water were charged in a round flask and stirred at room temperature overnight and extracted with hexane (3 x 100 mL). The organic phase was discarded and the aqueous phase was acidified with 4 M HCl until a pH value of 1 was achieved. The mixture was extracted with ethyl acetate for three times. The organic solution was washed with brine and dried over anhydrous magnesium sulfate, filtered and evaporation of solvent under reduced pressure yielded in a bluish oil (9.58 g, 50.63 mmol, 90.22 %).

(S)-2-[tert-butoxycarbonyl-methylamino]acetic acid (9.58 g, 50.63 mmol) was dissolved in dry CH_2Cl_2 under nitrogen atmosphere and PCl_3 was slowly added at 0°C. The mixture was stirred for 2 hours at room temperature and volatiles were removed under reduced pressure. The flask was transferred into the glovebox and residues were resuspended in dry CH_2Cl_2, a spatula tip-full of NaH was added and stirred for 30 minutes. After filtration and evaporation of the solvent, Me-NCA was precipitated in hexane. White crystals were formed, transferred into a sublimation device and purified by sublimation at 100 °C at 0.04 mbar yielding a white solid (2.87 g, 24.93 mmol, total yield: 44.43 %). Figure 46 shows the ^{1}H-NMR of M7 (see Table 1) with high purity.

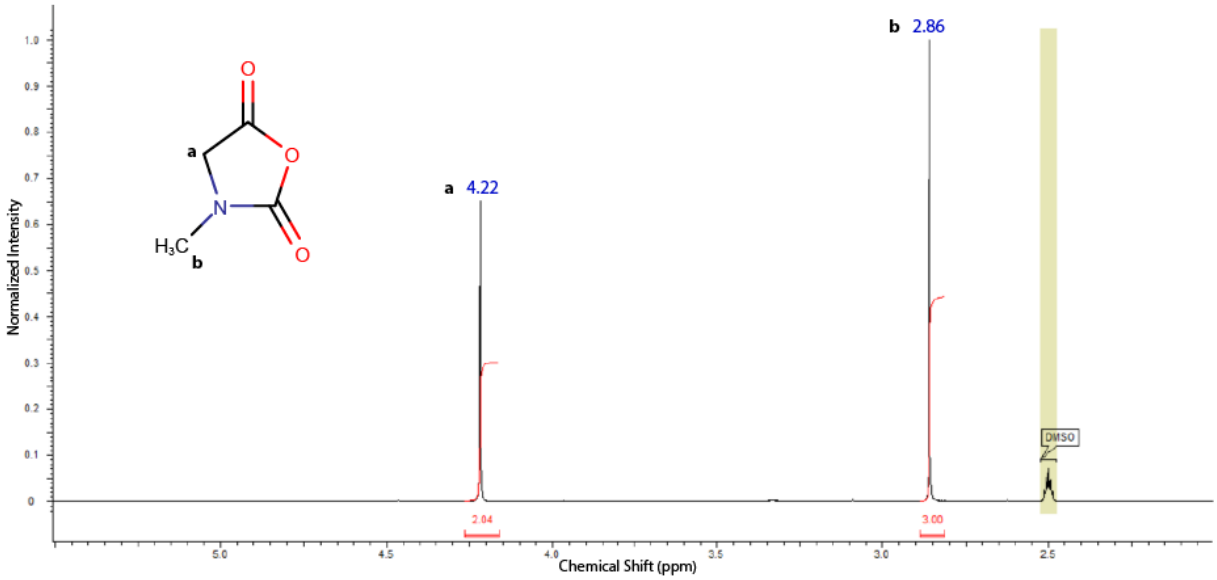

Figure 46: Me-NCA (M7): ^{1}H-NMR (300 MHz, DMSO, δ, ppm): 4.22 (s, 2H, NC*H*$_2$C(O)), 2.86 (s, 3H, C*H*$_3$).

6.3.3 *N*-Butyl-*N*-carboxyanhydride Synthesis Method A

Butylamine (6.14 g, 85.14 mmol) was added to 400 mL CH_2Cl_2 and glyoxylic acid (15.13 g , 204.40 mmol). The solution turned yellow and was stirred for 24 hours at room temperature. The solvent was evaporated and 400 mL of 1 M HCl was added to the remnant in the flask and heated under reflux for additional 24 hours. The aqueous solvent was evaporated, yielding in a yellowish solid. The residues were recrystallized in methanol/diethyl ether (1/5, v/v) to yield a white solid (7.35 g, 50.63 mmol, 59.47 %)

N-Butylglycine Hydrochloride (7.35 g, 50.63 mmol) was suspended in 70 mL toluene in a round flask. The glassware was put into in ice bath and cooled down to 0 °C. NaOH (6.20 g, 155.06 mmol) was dissolved in 70 mL Milli Q water and added to the mixture. Benzyl chloroformate (8.52 g, 49.95 mmol) was slowly added and the solution was stirred for 4 hours. After that the mixing was stopped, the organic phase was discarded and the aqueous phase was returned to the flask and acidified with 4 M HCl to a pH value of 1. After that the solution was extracted

with ethyl acetate (70 mL each) for three times. The organic phase was washed with brine and dried over anhydrous magnesium sulfate. The solvent was removed under reduced pressure yielding in slightly yellow oil (14.43 g, 50.63 mmol).

Acetyl chloride (8.11 g, 103.36 mmol) was added to 14.43 g *N*-benzyloxycarbonyl-*N*-butylglycine (50.63 mmol) and dissolved in acetic anhydride (10.37 g, 102.09 mmol) under dry nitrogen atmosphere. The mixture was heated up to 70 °C and refluxed for 6 hours. Solvent and excess of acetyl chloride were removed under reduced pressure under nitrogen atmosphere, yielding a crude oil. The crude oil could not be distilled, since the solvent hampered the fractionation (azeotropic mixture).

6.3.4 *N*-Butyl-*N*-carboxyanhydride Synthesis Method B

Butylamine (24.70 mL, 250.00 mmol), methyl bromacetate (28.4 mL, 299.86 mmol), Et_3N (38.30 mL, 274.76 mL) and 310 mL ethyl acetate were charged in a round bottom flask and stirred for 24 hours at 55 °C. White-yellow solids started to precipitate out. The aqueous layer was discarded and the organic phase was washed with brine, dried over anhydrous magnesium sulfate, filtered and the solvent was removed under reduced pressure, yielding in slightly yellow oil (34.46 g, 237.32 mmol, 94.93 %).

The yellowish oil was then acidified with HCl (1.3 L, 4 M) and stirred for 16 hours at 55 °C. The aqueous solvent was removed under reduced pressure, yielding yellow-white crystals. Recrystallization in methanol/diethyl ether at 0 °C yielded a white solid (23.27 g, 177.40 mmol, 90.09 %).

(S)-2-(1-phenylbutylamino)acetic acid hydrochloride (23.27 g, 177.4 mmol), Boc_2O (96.90 mL, 443.99 mmol), Et_3N (123.40 mL, 1216.00 mmol) and 720 mL Milli Q water were charged in a round flask and stirred at room temperature for 16 hours and extracted with hexane (3 x 100 mL). The organic phase was discarded and the aqueous phase was acidified with 4 M HCl until a pH value of 1 was achieved. The mixture was extracted with ethyl acetate for three times. The organic solution was washed with brine and dried over anhydrous magnesium sulfate, filtered and evaporation of solvent under reduced pressure yielded a yellowish oil (26.33 g, 113.83 mmol, 64.17 %).

(S)-2-[tert-butoxycarbonyl-butylamino]acetic acid (26.33 g, 113.83 mmol) was dissolved in 580 mL dry CH_2Cl_2 under nitrogen atmosphere and PCl_3 (11.90 mL, 136.42 mmol) was slowly added at 0°C. The mixture was stirred for 2 hours at room temperature and volatiles were removed under reduced pressure. The flask was transferred into the glovebox and residues were

resuspended in dry CH_2Cl_2, a spatula tip-full of NaH was added and stirred for 30 minutes. After filtration and evaporation of the solvent, Bu-NCA was distilled at 100 °C at 0.04 mbar yielding in a colorless, oil (12.27 g, 78.07 mmol, yield: 31.23 %).

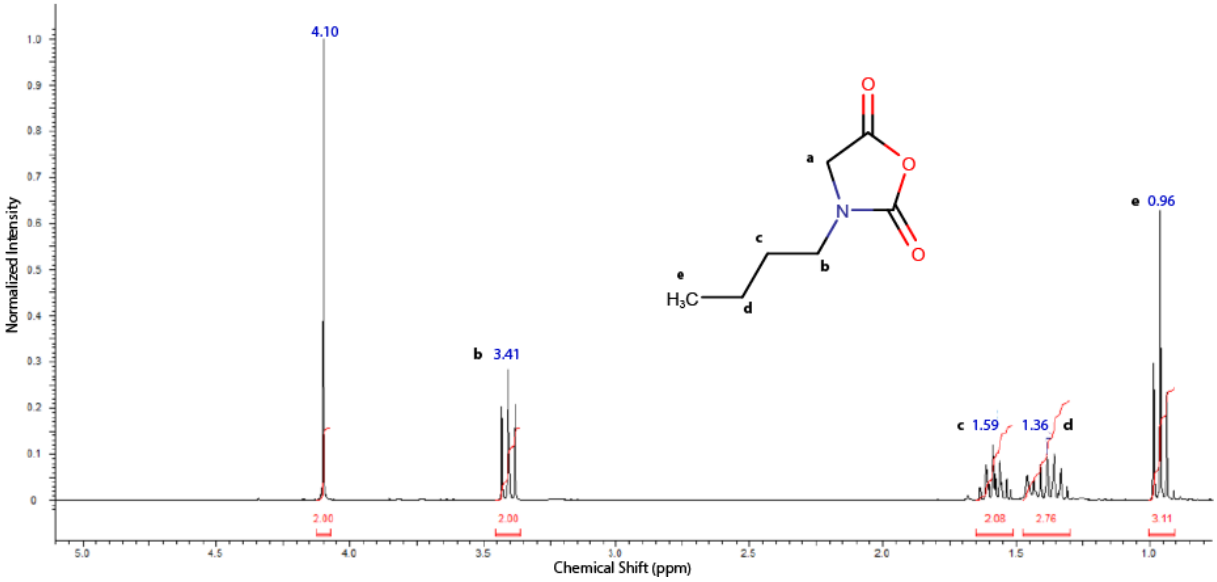

Figure 47: Bu-NCA (see Table 1, entry M13): ^{1}H NMR (300 MHz, $CHCl_3$, δ, ppm): 4.10 (s, 2H, $NCH_2C(O)$), 3.41 (t, 2H, NCH_2CH_2), 1.59 (quin, 2H, $CH_2CH_2CH_2$), 1.38 (qt, 2H, CH_2CH_3), 0.96 (t, 3H, CH_3).

6.3.5 *N*-Ethyl-*N*-carboxyanhydride Synthesis Method B

2 M Ethylamine in THF (150.00 mL, 300.00 mmol), methyl bromacetate (34.00 mL, 335.19 mmol), Et_3N (46.20 mL, 331.43 mmol) and 270 mL ethyl acetate were charged in a round bottom flask and stirred for 30 hours at 55 °C. A white solid started to precipitate out. The aqueous layer was discarded and the organic phase was washed with brine, dried over anhydrous magnesium sulfate, filtered and the solvent was removed under reduced pressure, yielding in a clear oil (22,59 g, 192.83 mmol, 64.30 %).

The oil was acidified with 955 mL 4 M HCl and stirred for 16 hours at 55 °C. The solution stayed clear, but turned to an orange-brown color. The aqueous solvent was removed under reduced pressure, yielding orange-brown crystals. Recrystallization was carried out in methanol/THF (1/5, v/v) at -20 °C. A yield of white-orange solids (16.50 g, 160.00 mmol, 82.97%) was obtained.

(S)-2-(1-phenylethylamino)acetic acid hydrochloride (16.50 g, 160.00 mmol), Boc_2O (101.04 mL , 440.03 mmol), Et_3N (140.22 mL, 1379.58 mmol) and 600 mL Milli Q water were charged in a round flask and stirred at room temperature overnight and extracted with hexane (3 x 100 mL). The organic phase was discarded and the aqueous phase was acidified with 4 M HCl until a pH value of 1 was achieved. The mixture was extracted with ethyl acetate for three times. The

organic solution was washed with brine and dried over anhydrous magnesium sulfate, filtered and evaporation of solvent under reduced pressure yielded in a yellowish oil (6.23 g, 30.24 mmol, 18.90 %).

(S)-2-[tert-butoxycarbonyl-ethylamino]acetic acid (6.23 g, 30.24 mmol) was dissolved in 70 mL dry CH_2Cl_2 under nitrogen atmosphere and PCl_3 (1.75 mL, 31.76 mmol) was slowly added at 0 °C. The mixture was stirred for 2 hours at room temperature and volatiles were removed under reduced pressure. The flask was transferred into the glovebox and residues were resuspended in dry CH_2Cl_2, a spatula tip-full of NaH was added and stirred for 30 minutes. After filtration and evaporation of the solvent, Et-NCA was tried to be distilled at 100 °C at 0.04 mbar, but no product could be isolated, since the product was too viscous.

6.4 Polymer Synthesis

All samples were polymerized in a GS glovebox (water level ≤1 ppm, oxygen level ≤10 ppm). Sealable Glass vials equipped with a magnetic stirring bar were charged with DMSO, NMP and placed in heating block at 22 or 50 °C. Next Bu- and Me-NCA were added to the reaction mixture. The initiator – nitrodopamine-modified SPIONs – was added to the mixture and started the reaction. The individual composition of the samples is listed in Table 6.

Table 6: Chemical composition of surface-grafted polypeptoid.

Sample	**SPION[a]**		**Me-NCA**		**Bu-NCA**		**[M/I]**
	m [mg]	**n [mmol]**	**m [mg]**	**n [mmol]**	**m [mg]**	**n [mmol]**	
P1	8.8	0.013	184	1.60	216	1.37	200
P2	8.8	0.013	200	1.74	200	1.27	200
P3	17.6	0.026	204	1.77	200	1.27	100
P4	8.8	0.013	234	2.03	166	1.05	200
P5	17.6	0.026	220	1.91	180	1.14	100
P6	35.2	0.052	225	1.96	176	1.12	50

[a] used for surface-initiated co-polymerization (NDA-coated SPION). Each sample was dissolved in 5.3 ml DMSO with 300 µL (3.1 mmol) NMP.

The polymerization was stopped after 72 hours by precipitation with adding diethyl ether. The supernatant of the polypeptoid-grafted SPION was discarded by magnetic decantation, particles were redispersed in DMF and precipitated again in diethyl ether. Before freeze drying, the SPION samples were dialyzed against water for 24 hours (MWCO: 100 kDa) to remove free polymer.

7 REFERENCES

1. Buzea, C., I.I. Pacheco, and K. Robbie, *Nanomaterials and nanoparticles: Sources and toxicity.* Biointerphases, 2007. **2**(4): p. MR17.
2. Stuart, D.A., et al., *Biological applications of localised surface plasmonic phenomenae.* IEE Proc Nanobiotechnol, 2005. **152**(1): p. 13-32.
3. Moeller, R. and W. Fritzsche, *Chip-based electrical detection of DNA.* IEE Proc Nanobiotechnol, 2005. **152**(1): p. 47-51.
4. Van Aert, S., et al., *Three-dimensional atomic imaging of crystalline nanoparticles.* Nature, 2011. **470**(7334): p. 374-7.
5. Dai, S., P. Ravi, and K.C. Tam, *pH-Responsive polymers: synthesis, properties and applications.* Soft Matter, 2008. **4**(3): p. 435.
6. Dai, S., P. Ravi, and K.C. Tam, *Thermo- and photo-responsive polymeric systems.* Soft Matter, 2009.
7. Zhang, J. and R.D. Misra, *Magnetic drug-targeting carrier encapsulated with thermosensitive smart polymer: core-shell nanoparticle carrier and drug release response.* Acta Biomater, 2007. **3**(6): p. 838-50.
8. Ghosh Chaudhuri, R. and S. Paria, *Core/shell nanoparticles: classes, properties, synthesis mechanisms, characterization, and applications.* Chem Rev, 2012. **112**(4): p. 2373-433.
9. Amstad, E., M. Textor, and E. Reimhult, *Stabilization and functionalization of iron oxide nanoparticles for biomedical applications.* Nanoscale, 2011. **3**(7): p. 2819-43.
10. R. Weissleder, P.F.H., D. D. Stark, E. Rummeny, S. Saini, J. Wittenberg and J. T. Ferrucci, *Superparamagnetic Iron Oxide: Clinical Application as a Contrast Agent for MR Imaging of the Liver.* Abdominal and Gastrointestinal Radiology, 1987. **168**: p. 297-301.
11. Mahmoudi, M., et al., *Superparamagnetic iron oxide nanoparticles (SPIONs): development, surface modification and applications in chemotherapy.* Adv Drug Deliv Rev, 2011. **63**(1-2): p. 24-46.
12. Benz, M., *Superparamagnetism: Theory and Applications*. 2012, ETH Zürich.
13. F. Hasany, S., et al., *Systematic Review of the Preparation Techniques of Iron Oxide Magnetic Nanoparticles.* Nanoscience and Nanotechnology, 2013. **2**(6): p. 148-158.
14. Park, J., et al., *One-nanometer-scale size-controlled synthesis of monodisperse magnetic iron oxide nanoparticles.* Angew Chem Int Ed Engl, 2005. **44**(19): p. 2873-7.
15. Bixner, O., et al., *Complete Exchange of the Hydrophobic Dispersant Shell on Monodisperse Superparamagnetic Iron Oxide Nanoparticles.* Langmuir, 2015. **31**(33): p. 9198-204.
16. Esther Amstad, T.G., Idalia Bilecka, Marcus Textor, Erik Reimhult, *Ultrastable Iron Oxide Nanoparticle Colloidal Suspensions Using Dispersants with Catechol-Derived Anchor Groups.* Nano Letters, 2009. **9**(12): p. 4042-4048.
17. Yuen, A.K., et al., *The interplay of catechol ligands with nanoparticulate iron oxides.* Dalton Trans, 2012. **41**(9): p. 2545-59.
18. Rodenstein, M., et al., *Fabricating chemical gradients on oxide surfaces by means of fluorinated, catechol-based, self-assembled monolayers.* Langmuir, 2010. **26**(21): p. 16211-20.

19. Borase, T. and A. Heise, *Hybrid Nanomaterials by Surface Grafting of Synthetic Polypeptides Using N-Carboxyanhydride (NCA) Polymerization.* Adv Mater, 2016. **28**(27): p. 5725-31.
20. Zhang, D., et al., *Polypeptoid Materials: Current Status and Future Perspectives.* Macromolecules, 2012. **45**(15): p. 5833-5841.
21. Byrne, M., et al., *Star-Shaped Polypeptides: Synthesis and Opportunities for Delivery of Therapeutics.* Macromol Rapid Commun, 2015.
22. al., R.N.Z.e., *Sequence-specific polypeptoids: A diverse family of heteropolymers with stable secondary structure.* Proc. Natl. Acad. Sci. USA, 1998. **95**: p. 4303 - 4308.
23. Tran, H., et al., *Solid-phase submonomer synthesis of peptoid polymers and their self-assembly into highly-ordered nanosheets.* J Vis Exp, 2011(57): p. e3373.
24. Kurzhals, S., R. Zirbs, and E. Reimhult, *Synthesis and Magneto-Thermal Actuation of Iron Oxide Core-PNIPAM Shell Nanoparticles.* ACS Appl Mater Interfaces, 2015. **7**(34): p. 19342-52.
25. Diehl, C. and H. Schlaad, *Thermo-responsive polyoxazolines with widely tuneable LCST.* Macromol Biosci, 2009. **9**(2): p. 157-61.
26. Lahasky, S.H., et al., *Synthesis and characterization of thermo-responsive polypeptoid bottlebrushes.* Polym. Chem., 2014. **5**(4): p. 1418-1426.
27. Fetsch, C., et al., *Polypeptoids from N-Substituted GlycineN-Carboxyanhydrides: Hydrophilic, Hydrophobic, and Amphiphilic Polymers with Poisson Distribution.* Macromolecules, 2011. **44**(17): p. 6746-6758.
28. Brittain, W.J. and S. Minko, *A structural definition of polymer brushes.* Journal of Polymer Science Part A: Polymer Chemistry, 2007. **45**(16): p. 3505-3512.
29. M. Tirrell, S.P., G. Hadziioannou, *Polymeric amphiphiles at solid-fluid interfaces: Forces between layers of adsorbed block copolymers.* Proc. Natl. Acad. Sci. USA, 1987. **84**: p. 4725-4728.
30. Lau, K.H., et al., *Surface-grafted polysarcosine as a peptoid antifouling polymer brush.* Langmuir, 2012. **28**(46): p. 16099-107.
31. Nikos Hadjichristidis, H.I., Marinos Pitsikalis, Georgios Sakellariou, *Synthesis of Well-Defined Polypeptide-Based Materials via the Ring-Opening Polymerization of a-Amino Acid N-Carboxyanhydrides.* Chemical Reviews, 2009. **109**(11): p. 5528–5578.
32. Wibowo, S.H., et al., *Polypeptide films via N-carboxyanhydride ring-opening polymerization (NCA-ROP): past, present and future.* Chem Commun (Camb), 2014. **50**(39): p. 4971-88.
33. Babu, K. and R. Dhamodharan, *Synthesis of Polymer Grafted Magnetite Nanoparticle with the Highest Grafting Density via Controlled Radical Polymerization.* Nanoscale Res Lett, 2009. **4**(9): p. 1090-102.
34. Ricardo Amils, J.C.Q., Henderson James (Jim) Cleaves II, William M. Irvine, Daniele L. Pinti and Michel Viso, *Encyclopedia of Astrobiology,* M. Gargaud, Editor. 2011, Springer: Heidleberg. p. 80 - 82.
35. Leuchs, H., *Ueber die Glycin-carbonsäure.* Ber. Dtsch. Chem. Ges., 1906. **39**: p. 857–861.
36. Guo, L., et al., *Synthesis and characterization of cyclic and linear helical poly(α-peptoid)s by N-heterocyclic carbene-mediated ring-opening polymerizations of N-substituted N-carboxyanhydrides.* Biopolymers, 2011. **96**(5): p. 596-603.
37. Antony W. Burgess, Y.P., Sydney J. Leach, *The Random Coil Dimensions of Methylated Polypeptides.* Journal of Polymer Science, 1975. **49**: p. 75 - 83.
38. Deming, T.J., *Facile synthesisof block copolypeptides of defined architectur.* Nature, 1997. **390**: p. 386 - 389.
39. Dimitrov, I. and H. Schlaad, *Synthesis of nearly monodisperse polystyrene–polypeptide block copolymers via polymerisation of N-carboxyanhydrides.* Chem. Commun., 2003(23): p. 2944-2945.

40. Thrasyvoulos Aliferis, H.I., and Nikos Hadjichristidis, *Living Polypeptides.* Biomacromolecules, 2004. **5**: p. 1653 - 1656.
41. Nuyken, O. and S. Pask, *Ring-Opening Polymerization—An Introductory Review.* Polymers, 2013. **5**(2): p. 361-403.
42. al., S.H.T.e., *Living Free-Radical Polymerization by Reversible Addition.* Macromolecules, 1998. **31**: p. 5559-5562.
43. Kralingen, L.v., *Controlled Polymerization of Amino acid Derivatives*. 2008, Stellenbosch University.
44. Masahiko Sisido, Y.I., Toshinobu Higashimura, *Molecular Weight Distribution of Polysarcosine Obtained by NCA Polymerization.* Makromol. Chem., 1977. **178**: p. 3107 - 3114.
45. Tao, X., et al., *Polypeptoids with tunable cloud point temperatures synthesized from N-substituted glycine N-thiocarboxyanhydrides.* Polym. Chem., 2015. **6**(16): p. 3164-3174.
46. Zirbs, R., et al., *Melt-grafting for the synthesis of core-shell nanoparticles with ultra-high dispersant density.* Nanoscale, 2015. **7**(25): p. 11216-25.
47. Hans R. Kricheldorf, C.v.L., Gert Schwarz, *Cyclic Polypeptides by Solvent-Induced Polymerizations of R-Amino Acid N-Carboxyanhydrides.* Macromolecules 2005(38): p. 5513-5518.
48. Guo, L., et al., *N-Heterocyclic carbene-mediated zwitterionic polymerization of N-substituted N-carboxyanhydrides toward poly(alpha-peptoid)s: kinetic, mechanism, and architectural control.* J Am Chem Soc, 2012. **134**(22): p. 9163-71.
49. Lahasky, S.H., X. Hu, and D. Zhang, *Thermoresponsive Poly(α-peptoid)s: Tuning the Cloud Point Temperatures by Composition and Architecture.* ACS Macro Letters, 2012. **1**(5): p. 580-584.

ABBREVIATIONS

Boc_2O – di-*tert*-butyldicarbonate
BOKU – University of Natural Resources and Life Sciences, Vienna
Bu-NCA – *N*-Butyl *N*-carboxyanhydride
CH_2Cl_2 – dichloromethane
CSNP – core-shell nanoparticle
DLS – dynamic light scattering
DMSO – dimethyl sulfoxide
Et-NCA – *N*-Ethyl *N*-carboxyanhydride
GA – glyoxylic acid
LCST– lower critical solution temperature
LiTFA – lithium trifluoracetate
MALDI-TOF – matrix-assisted laser desorption/ionization time of flight mass spectra
Me-NCA – *N*-Methyl *N*-carboxyanhydrde
MW – molecular weight
NaH – sodium hydride
NCA – *N*-carboxyanhydride
NMP – *N*-Methyl-2-pyrrolidone
NP – nanoparticle
OA – oleic acid
PAA – poly(acrylic acid)
PDI – polydispersity index
ROP – ring-opening polymerization
SPION – superparamagnetic iron oxide nanoparticle
T_{CP} – cloud point temperature
TEM – transmission electron microscopy
TGA – thermogravimetric analysis